Probing long-lived doubly charged scalar in the Georgi-Machacek model at the LHC and in far detectors

Chih-Ting Lu,* Xinyu Wang,† Xinqi Wei,‡ and Yongcheng Wu§

Department of Physics and Institute of Theoretical Physics,

Nanjing Normal University, Nanjing, 210023, China

(Dated: November 19, 2024)

Searching for long-lived particles (LLPs) beyond the Standard Model (SM) is a promising direction in collider experiments. The Georgi-Machacek (GM) model extends the scalar sector in the SM by introducing various new scalar bosons. In this study, we focus on the parameter space that allows the light doubly charged scalar to become long-lived. This light doubly charged scalar is fermophobic and predominantly decays into a pair of on-shell or off-shell same-sign W bosons. We investigate three types of signal signatures at the LHC: displaced vertices in the inner tracking detector, displaced showers in the muon system, and heavy stable charged particles. Additionally, we analyze the potential for detecting such doubly charged scalars in far detectors, including ANUBIS, MATHUSLA, FACET, FASER, CODEX-b, MoEDAL-MAPP and AL3X. By combining the LLP searches at the LHC and in far detectors, we project that the limits on the mixing angle, θ_H , (between the doublet and triplets) can cover most of the parameter space with $\sin \theta_H \lesssim 10^{-3}$ for the mass range of long-lived doubly charged scalars between 50 GeV to 180 GeV, assuming the full integrated luminosity at the LHC and HL-LHC.

^{*} ctlu@njnu.edu.cn

[†] xinyuwang@njnu.edu.cn

[‡] xqwei@njnu.edu.cn

[§] ycwu@njnu.edu.cn

CONTENTS

I.	Introduction	3
II.	The Georgi-Machacek model	5
	A. Model setup and low-mass benchmark	5
	B. The production and decay of $H_5^{\pm\pm}$	10
	1. The pair production of $H_5^{\pm\pm}$	10
	2. The decay of $H_5^{\pm\pm} \to W^{\pm}W^{\pm}$	12
III.	Searching for the long-lived $H_5^{\pm\pm}$ at the LHC and in far detectors	14
	A. $H_5^{\pm\pm}$ decays within the inner tracking detector	16
	B. $H_5^{\pm\pm}$ decays within the muon system	19
	C. $H_5^{\pm\pm}$ as a heavy stable charged particle	22
	D. $H_5^{\pm\pm}$ decays in far detectors	24
IV.	Conclusion	26
	Acknowledgments	29
Α.	Trajectories of particles affected by magnetic fields in the LHC detectors	29
	References	30

I. INTRODUCTION

Searching for new scalar bosons beyond the Standard Model (SM) is an important mission at the Large Hadron Collider (LHC) and future colliders. Some simple extensions of the scalar sector in the SM include scalar singlet models [1, 2], two-Higgs doublet models (2HDM) [3–5], scalar triplet models [6, 7], and the Georgi-Machacek (GM) model [8–20], among others. The GM model is particularly notable for providing rich phenomenological predictions at collider experiments [21–26], neutrino experiments [27], and gravitational wave experiments [28, 29]. Moreover, the GM model can explain some experimental anomalies, including the excess of 95 GeV signal in $\gamma\gamma$, $b\bar{b}$, $\tau\tau$ channels [30]. In the GM model, the CP-even singlet as well as the triplet and fiveplet scalars can all be used as candidates for the mass with 95 GeV to explain this possible excess.

The GM model introduces extra complex and real triplets in addition to the SM particles, which ensures the preservation of custodial symmetry at tree level. After electroweak symmetry breaking (EWSB), the GM model includes a fiveplet, two triplets, and two singlets where one of the singlets will be identified as the SM-like Higgs boson with the mass of 125 GeV, one of the triplets corresponds to the goldstone. The extra triplet and singlet are similar to those in the 2HDM, which have been searched for in many channels 31-41. For the fiveplet, the searches mainly focus on the charged components especially the doubly charged component. In general, several channels have been probed for a general doubly charged scalar, including the Drell-Yan production [42], vector-boson-fusion (VBF) process [22, 43, 44] and those involving lepton number violation at the LHC [45–48] as well as the production from ep collision at HERA [49] and e^+e^- collision at LEP [50–53]. However, the searches involving the lepton number violation interaction are not applicable to the doubly charged component of the fiveplet in GM model, as the fiveplet is fermiophobic at tree-level. Hence the most relevant ones are those where the doubly charged scalar is produced and decaying through its coupling with gauge bosons. For the same reason, the single charged fivplet is also mainly searched through its coupling with gauge boson utilizing the VBF production and associated production with other fiveple and the decay channels to gauge bosons [21, 23, 25, 42]. The coupling between the fiveplet and the gauge bosons is proportional to the triplet vacuum expectation value (vev). In general, suppression of the contribution from the triplet vev to the total one will not affect those analysis based on its gauge couplings. However, when the triplet vev is highly suppressed, as well as when the mass of fiveplet is below the decay threshold of two on-shell gauge bosons, the decay length of $H_5^{\pm\pm}$ will increase, it may become long-lived particle (LLP) which alters the analysis based on the gauge boson final states. The current analysis hence loss its sensitivity in such low mass and low triplet vev region. In this work, we will focus on the parameter region where $H_5^{\pm\pm}$ is long-lived.

Due to their distinct experimental signatures, LLPs play a crucial role in the search for new physics beyond the SM. LLPs can travel significant distances within a detector before decaying, producing observable phenomena such as displaced vertices or unusual energy deposits that may be missed by traditional searches focused on prompt decays. These unique characteristics make LLPs invaluable for probing new physics, particularly in parameter regions that are otherwise difficult to access. In the GM model, the $H_5^{\pm\pm}$ can become an LLP under certain conditions, such as when the triplet vev is highly suppressed or when its mass is below the threshold for decays into two on-shell same-sign W bosons. Studying LLPs enhances the experimental sensitivity at the LHC, enabling exploration of new parameter spaces and providing deeper insights into the mechanisms of electroweak symmetry breaking and the structure of scalar sectors.

The main focus of this work is the search for the long-lived $H_5^{\pm\pm}$ in the GM model at the LHC and far detectors¹. If the charged LLPs have lifetimes sufficient to travel detectable distances within the detector before decaying, several general searches can be conducted at the LHC and in far detectors:

- Inner tracking detector: LLPs travel a measurable distance before decaying, leading to displaced vertices within the inner tracking detector away from the primary collision point [58]. LLPs decaying into charged particles can leave tracks with large impact parameters relative to the primary vertex. Searches for events with such high-impact parameter tracks are carried out [59].
- Muon system: Some LLPs can traverse the electromagnetic calorimeter, hadronic calorimeter and decay into leptons and/or jets in the muon system, where they are reconstructed as a cluster-type signal, leaving distinctive signatures in the muon system. Searches for excesses of energetic clusters are conducted [60].

¹ There are some previous studies for the long-lived doubly charged scalars in Type-II seesaw model and Left-right symmetry model at the LHC [54–57].

- Tracking detectors: Some LLPs live long enough to fly out of the detectors, leaving a unique charged track signature inside the detectors, hence the name heavy stable charged particles (HSCPs).
- Far detectors: Near each collision point, several far detectors are under construction or in preparation, such as ANUBIS [61], MATHUSLA [62], FACET [63], FASER, FASER2 [64], CODEX-b [65], MoEDAL-MAPP [66] and AL3X [67]. Some LLPs have a sufficiently long lifetime to fly out of ATLAS/CMS/LHCb/ALICE detectors and reach these far detectors.

Therefore, we focus on the following four detector areas to search for long-lived $H_5^{\pm\pm}$: (1) Inner tracker system; (2) Muon system; (3) Heavy stable charged particles (HSCPs); (4) Far detectors (ANUBIS, MATHUSLA, FACET, FASER, CODEX-b, MoEDAL-MAPP and AL3X).

The rest of this paper is organized as follows. We briefly review the GM model and the production and decay of the doubly charged scalar in Sec. II, from which we will demonstrate the parameter region for long-lived $H_5^{\pm\pm}$. The search strategies and results for the long-lived doubly charged scalar at the LHC and in the far detectors are presented in Sec. III. Finally, we present our findings and discussions in Sec. IV.

II. THE GEORGI-MACHACEK MODEL

A. Model setup and low-mass benchmark

The scalar sector of GM model [8, 9] includes the usual Higgs doublet $\phi = (\phi^{\dagger}, \phi^0)^T$, and extra two triplets, one complex $\chi = (\chi^{++}, \chi^+, \chi^0)^T$ and one real $\xi = (\xi^+, \xi^0, -\xi^{+*})^T$. The fields are arranged in the form of bi-doublet and bi-triplet in order to make the global symmetry $SU(2)_L \times SU(2)_R$ manifest:

$$\Phi \equiv (\varepsilon_2 \phi^*, \phi) = \begin{pmatrix} \phi^{0*} & \phi^+ \\ -\phi^{+*} & \phi^0 \end{pmatrix}, \quad \text{with} \quad \varepsilon_2 = \begin{pmatrix} 0 & 1 \\ -1 & 0 \end{pmatrix}, \tag{1}$$

$$X \equiv (\varepsilon_3 \chi^*, \xi, \chi) = \begin{pmatrix} \chi^{0*} & \xi^+ & \chi^{++} \\ -\chi^{+*} & \xi^0 & \chi^+ \\ \chi^{++*} & -\xi^{+*} & \chi^0 \end{pmatrix}, \quad \text{with} \quad \varepsilon_3 = \begin{pmatrix} 0 & 0 & 1 \\ 0 & -1 & 0 \\ 1 & 0 & 0 \end{pmatrix}. \tag{2}$$

The most general gauge invariant scalar potential involving Φ and X that is also preserving the global $SU(2)_L \times SU(2)_R$ can be written as [68]

$$V(\Phi, X) = \frac{\mu_2^2}{2} \text{Tr}(\Phi^{\dagger}\Phi) + \frac{\mu_3^2}{2} \text{Tr}(X^{\dagger}X) + \lambda_1 \left[\text{Tr}(\Phi^{\dagger}\Phi) \right]^2 + \lambda_2 \text{Tr}(\Phi^{\dagger}\Phi) \text{Tr}(X^{\dagger}X)$$
$$+ \lambda_3 \text{Tr}(X^{\dagger}XX^{\dagger}X) + \lambda_4 \left[\text{Tr}(X^{\dagger}X) \right]^2 - \lambda_5 \text{Tr}(\Phi^{\dagger}\tau^a\Phi\tau^b) \text{Tr}(X^{\dagger}t^aXt^b)$$
$$- M_1 \text{Tr}(\Phi^{\dagger}\tau^a\Phi\tau^b) (UXU^{\dagger})_{ab} - M_2 \text{Tr}(X^{\dagger}t^aXt^b) (UXU^{\dagger})_{ab}, \tag{3}$$

where the τ^i and t^i (i=1,2,3) correspond to the SU(2) generators for the doublet and triplet representations, respectively. $\tau^i = \sigma^i/2$ where σ^i are the Pauli matrices and t^i 's are given by

$$t^{1} = \frac{1}{\sqrt{2}} \begin{pmatrix} 0 & 1 & 0 \\ 1 & 0 & 1 \\ 0 & 1 & 0 \end{pmatrix}, \quad t^{2} = \frac{1}{\sqrt{2}} \begin{pmatrix} 0 & -i & 0 \\ i & 0 & -i \\ 0 & i & 0 \end{pmatrix}, \quad t^{3} = \begin{pmatrix} 1 & 0 & 0 \\ 0 & 0 & 0 \\ 0 & 0 & -1 \end{pmatrix}. \tag{4}$$

The matrix U is given by [69]

$$U = \begin{pmatrix} \frac{1}{\sqrt{2}} & 0 & \frac{1}{\sqrt{2}} \\ -\frac{i}{\sqrt{2}} & 0 & -\frac{i}{\sqrt{2}} \\ 0 & 1 & 0 \end{pmatrix}.$$
 (5)

Hence, in total, from the scalar potential, we have 9 free parameters of which μ_2^2 , μ_3^2 , M_1 and M_2 are dimensional and $\lambda_{1,\dots,5}$ are dimensionless.

The vacuum expectation values (vevs) of the bi-doublet Φ and the bi-triplet X are defined as

$$\langle \Phi \rangle = \frac{v_{\phi}}{\sqrt{2}} I_{2 \times 2}, \qquad \langle X \rangle = v_{\chi} I_{3 \times 3}, \tag{6}$$

where the vevs from both doublet and triplets contribute to the gauge boson mass giving rise to the constraint

$$v_{\phi}^2 + 8v_{\chi}^2 \equiv v^2 = \frac{1}{\sqrt{2}G_F} \approx (246 \,\text{GeV})^2.$$
 (7)

The real triplet ξ and the complex triplet χ are assumed to obtain the same vev, ie., $v_{\xi} = v_{\chi}$, to maintain the custodial SU(2)_C symmetry at tree-level. Further, the neutral fields are expanded around the corresponding vevs and decomposed into real and imaginary components according to

$$\phi^{0} = \frac{v_{\phi}}{\sqrt{2}} + \frac{\phi^{0,r} + i\phi^{0,i}}{\sqrt{2}}, \quad \chi^{0} = v_{\chi} + \frac{\chi^{0,r} + i\chi^{0,i}}{\sqrt{2}}, \quad \xi^{0} = v_{\chi} + \xi^{0}.$$
 (8)

The vevs of the doublet and triplets should minimize the potential by definition which provides the following two minimization conditions:

$$\frac{\partial V}{\partial v_{\phi}} = \left(\mu_2^2 + 4\lambda_1 v_{\phi}^2 + 6\lambda_2 v_{\chi}^2 - 3\lambda_5 v_{\chi}^2 - \frac{3}{2} M_1 v_{\chi}\right) v_{\phi} = 0,\tag{9}$$

$$\frac{\partial V}{\partial v_{\chi}} = 3\mu_3^2 v_{\chi} + 6\lambda_2 v_{\phi}^2 v_{\chi} + 12\lambda_3 v_{\chi}^3 + 36\lambda_4 v_{\chi}^3 - 3\lambda_5 v_{\phi}^2 v_{\chi} - \frac{3}{4} M_1 v_{\phi}^2 - 18M_2 v_{\chi}^2 = 0, \tag{10}$$

which will be used to replace μ_2^2 and μ_3^2 in terms of v_ϕ and v_χ as

$$\mu_2^2 = \frac{3}{2}M_1v_\chi - 4\lambda_1v_\phi^2 - 3(2\lambda_2 - \lambda_5)v_\chi^2,\tag{11}$$

$$\mu_3^2 = \frac{M_1 v_\phi^2}{4v_\chi} + 6M_2 v_\chi - 4(\lambda_3 + 3\lambda_4)v_\chi^2 - (2\lambda_2 - \lambda_5)v_\phi^2.$$
 (12)

The doublet and two triplets provide in total 13 physical fields. After electroweak symmetry breaking (EWSB), three of the fields correspond to the goldstone bosons, the rest are real physical fields which are arranged according to the representation under the custodial symmetry $SU(2)_C$ as two singlets, one triplet and one fiveplet. In terms of the original fields, the goldstone bosons are given by

$$G^{\pm} = c_H \phi^{\pm} + s_H \frac{\chi^{\pm} + \xi^{\pm}}{\sqrt{2}}$$

$$G^{0} = c_H \phi^{0,i} + s_H \chi^{0,i}$$
(13)

where we have defined

$$c_H \equiv \cos \theta_H = \frac{v_\phi}{v}, \quad s_H \equiv \sin \theta_H = \frac{2\sqrt{2}v_\chi}{v}.$$
 (14)

The physical fiveplet and triplet are given by

$$\begin{cases}
H_5^{\pm\pm} = \chi^{\pm\pm}, \\
H_5^{\pm} = \frac{\chi^{\pm} - \xi^{\pm}}{\sqrt{2}}, \\
H_5^{0} = \sqrt{\frac{2}{3}}\xi^{0} - \sqrt{\frac{1}{3}}\chi^{0,r},
\end{cases}$$

$$\begin{cases}
H_3^{\pm} = -s_H \phi^{\pm} + c_H \frac{\chi^{\pm} + \xi^{\pm}}{\sqrt{2}}, \\
H_3^{0} = -s_H \phi^{0,i} + c_H \chi^{0,i}.
\end{cases}$$
(15)

The masses of the fiveplet and triplet are given by, in terms of the quartic couplings in the potential and the vevs,

$$m_5^2 = 8\lambda_3 v_\chi^2 + \frac{3}{2}\lambda_5 v_\phi^2 + \frac{M_1}{4v_\chi} v_\phi^2 + 12M_2 v_\chi, \tag{16}$$

$$m_3^2 = \left(\frac{M_1}{4v_\chi} + \frac{\lambda_5}{2}\right)v^2. {17}$$

The two singlets in the gauge basis are given by

$$H_1^0 = \phi^{0,r},\tag{18}$$

$$H_1^{0'} = \sqrt{\frac{1}{3}}\xi^0 + \sqrt{\frac{2}{3}}\chi^{0,r}.$$
 (19)

The mass matrix in the gauge basis $(H_1^0, H_1^{0'})$ is given by

$$\mathcal{M}^2 = \begin{pmatrix} \mathcal{M}_{11}^2 & \mathcal{M}_{12}^2 \\ \mathcal{M}_{12}^2 & \mathcal{M}_{22}^2 \end{pmatrix}$$
 (20)

with

$$\mathcal{M}_{11}^2 = 8\lambda_1 v_\phi^2,\tag{21}$$

$$\mathcal{M}_{12}^2 = \frac{\sqrt{3}}{2} \left(4(2\lambda_2 - \lambda_5)v_\chi - M_1 \right) v_\phi, \tag{22}$$

$$\mathcal{M}_{22}^2 = \frac{M_1 v_\phi^2}{4v_\chi} - 6M_2 v_\chi + 8(\lambda_3 + 3\lambda_4) v_\chi^2. \tag{23}$$

These two singlets will thus further mix with each other to provide the mass eigenstates

$$h = \cos \alpha H_1^0 - \sin \alpha H_1^{0'}, \tag{24}$$

$$H = \sin \alpha H_1^0 + \cos \alpha H_1^{0'}. \tag{25}$$

The corresponding masses are m_h and m_H where we always assume that h is the SM-like Higgs. The mixing angle α is hence uniquely determined by the mass matrix in Eq. (20) with the above assumption. In the following analysis, we will always using $m_h = 125 \,\text{GeV}$ as one of the input parameters to facilitate the matching with current measurements at the LHC. We hence focus on the low- m_5 as well as low- s_H region for $H_5^{\pm\pm}$.

In GM model, the search strategies for the extra singlet and triplet are similar to that for the extra heavy scalars in 2HDM with corresponding scaling according to the couplings with SM gauge bosons and fermions. On the other hand, the fiveplet in GM model is fermiophobic, it has no couplings with fermions as it contains only the $SU(2)_L \times SU(2)_R$ triplet components ². The coupling of the fiveplet with gauge boson at tree-level is proportional to $s_H = 2\sqrt{2}v_\chi/v$. An important search strategy for the fiveplet focuses primarily on the doubly charged components, produced via Drell-Yan and vector boson fusion processes,

² However, in Type-II seesaw, the scalar triplet can have Yukawa couplings with the leptons [70]. In this analysis, we don't consider such scenario.

Fixed SM Parameters	Variable Parameters	Other Parameters in the Potential
$G_F = 1.1663787 \times 10^{-5} \mathrm{GeV}^{-2}$	$m_5 \in (50, 180) \mathrm{GeV}$	$\lambda_3 = -\lambda_4 = -1.5$
$m_h = 125 \mathrm{GeV}$	$s_H \in (10^{-9}, 10^{-2})$	$\lambda_5 = -4\lambda_2 = -0.32(m_5/100 \text{GeV})$
		$M_2 = 10 \mathrm{GeV}$

TABLE I. The low- m_5 benchmark for the GM model [73], with emphasis on low- s_H region.

and their subsequent decay into gauge bosons [42, 44]³. Note that, for the general doubly charged Higgs, there are actually two important decay modes, one is decaying into leptons for low triplet vev, and the other is decaying into W boson pair for high triplet vev [71, 72]. However due to its fermiophobic nature, those only involving couplings with gauge bosons are the relevant ones. Current LHC searches focus on the region where $m_5 \geq 200 \,\text{GeV}$ and can cover the parameter space up to $m_5 \lesssim 350 \,\text{GeV}$. However, these search do not extend to the lower mass region. Due to the large Drell-Yan pair production cross section in the low mass region, which does not scale with s_H , and the unique decay channel $H_5^{\pm\pm} \to W^{\pm}W^{\pm}$ (assuming other scalars are heavy, a natural assumption under current LHC searches), one might expect that this channel could easily cover the lower mass region. However, in this region, there is a special scenario where the above searches base on $H_5^{\pm\pm} \to W^{\pm}W^{\pm}$ could fail. If a small s_H suppresses the corresponding decay width, $H_5^{\pm\pm}$ may become a LLP, and the signatures would be significantly different from the usual multi-gauge bosons searches.

The most relevant parameters in the GM model for this scenario are the mass of the fiveplet m_5 which determines the kinematics and s_H which determines the decay length $c\tau$ of $H_5^{\pm\pm}$. Other parameters are irrelevant at leading order as long as the triplet are heavier than the fiveplet. Hence, in general, we have freedom to choose other model parameters and only focus on the m_5 - s_H parameter space plane. Here, for convenient, we choose the low- m_5 benchmark from [73] where the possible constraints in the m_5 - s_H plane are also discussed. Although some constraints become irrelevant when $H_5^{\pm\pm}$ becomes long-lived, the most significant constraint still arises from $H_5^0 \to \gamma\gamma$, depending on the specifics of the parameter space, as we will discuss below. The choice of model parameters in low- m_5 benchmark are given in Tab. I, where we have an emphasize on the low- s_H region by scanning in log-scale.

³ A deviation from the SM has been observed for a resonant $H_5^{\pm\pm}$ mass near 375 GeV, with a local (global) significance of 3.3 (2.5) standard deviations, as reported in Ref. [44]. Further data is required to verify this excess.

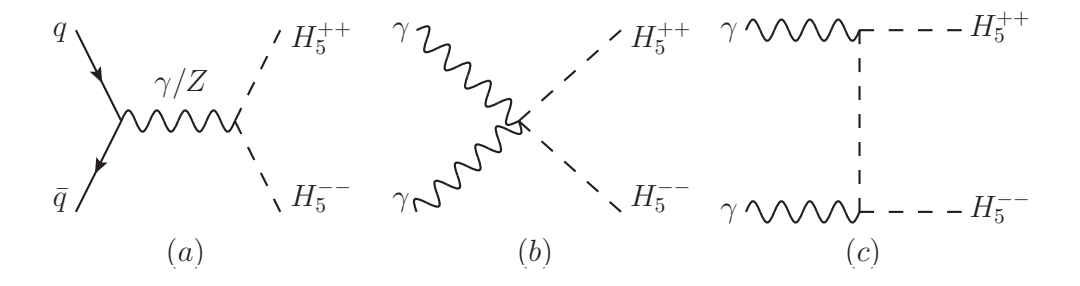


FIG. 1. The Feynman diagrams for the pair production of $H_5^{\pm\pm}$ including the Drell-Yan channel (a) and photon initiated channel (b, c and corresponding u-channel diagram).

Instead of using the parameters in the potential $(\mu_2^2, \mu_3^2, \lambda_{1,\dots,5}, M_1, M_2)$, this benchmark uses $(v, s_H, \lambda_{2,\dots,5}, M_2, m_h, m_5)$ where λ_1 is fixed by m_h given the singlet masses relation, M_1 is fixed by m_5 according to Eq. (16). Note that, the whole parameter space defined by low- m_5 benchmark is also subjected to the theoretical constraints which is included through GMCALC [74]. However, we emphasize again that the following analysis depends only on m_5 and s_H , the other parameters can be tuned as long as we have $m_5 < m_3$. Before we go into detail analysis of the signatures from long-lived $H_5^{\pm\pm}$, we discuss its production and decay in the rest of this section.

B. The production and decay of $H_5^{\pm\pm}$

1. The pair production of $H_5^{\pm\pm}$

The production of $H_5^{\pm\pm}$ is dominated by Drell-Yan pair production at low-mass region followed by photon initiated channel. The diagrams for these channels are shown in Fig. 1. The couplings in GM model involved in the production are the couplings between $H_5^{\pm\pm}$ and the γ/Z gauge bosons. The corresponding Feynman rules are given by

$$g_{H_5^{++}H_5^{--}\gamma} = -2ie(p_{H_5^{++}} - p_{H_5^{--}})^{\mu}, \qquad g_{H_5^{++}H_5^{--}Z} = 2ie\frac{c_{2W}}{s_{2W}}(p_{H_5^{++}} - p_{H_5^{--}})^{\mu},$$

$$g_{H_5^{++}H_5^{--}\gamma\gamma} = 8ie^2g^{\mu\nu}, \tag{26}$$

where it is important to notice that all these couplings are not suppressed by s_H . Hence, the cross section of these production channels do not depend on s_H . The cross sections of these production channels as functions of the mass are shown in Fig. 2 for different beam configurations. The cross sections are obtained using MadGraph5 [75] with the UFO model file

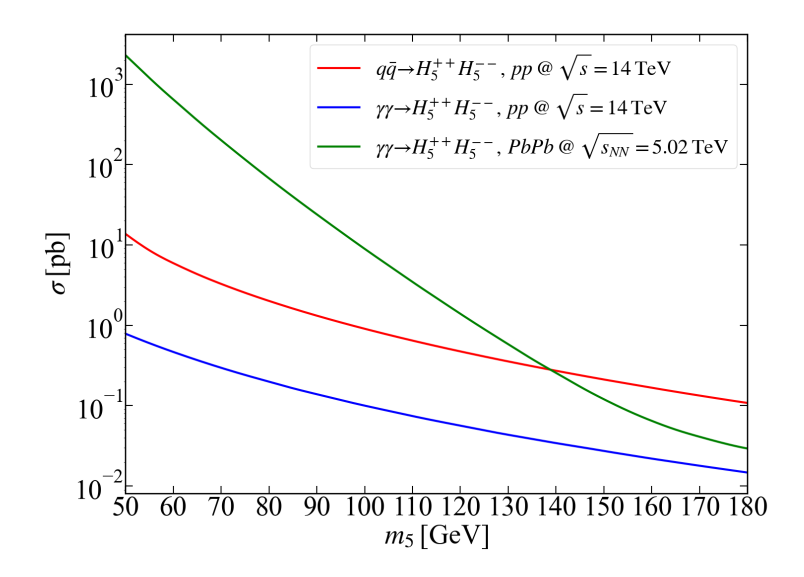


FIG. 2. The cross section for pair production of $H_5^{\pm\pm}$ as function of its mass m_5 including the Drell-Yan production channel (solid red) and photon initiated channel (solid blue) from p-p collision, as well as the photon initiated channel from Pb-Pb collision (solid green).

provided by [76] and the parameter card generated from GMCALC [74]. For the proton collision, NNPDF 3.1 [77, 78] including LUXqed formalism for the photon PDF [79, 80] is used. While for heavy-ion collision, the photon flux in ultraperipheral collision incorporated in MadGraph5 are used [81]. From proton collision, the Drell-Yan pair production is the dominant channel that can reach $\mathcal{O}(1)$ pb at low- m_5 region. The photon initiated channel including both elastic and inelastic contribution is subdominant and provides $\lesssim 10\%$ corrections. From a simple estimation, the contribution from elastic photon production in heavy-ion collisions will be enhanced by Z^4 , where Z is the proton number of the ion. In Fig. 2, we also show the cross section of such contribution from Pb-Pb collision with $\sqrt{s_{NN}}=5.02\,\mathrm{TeV}$. When the mass of $H_5^{\pm\pm}$ is small, the cross section is significantly enhanced. However, at higher mass regions, the cross section is greatly suppressed due to phase space limitations. Additionally, given the relatively low luminosity of Pb-Pb collision, this process is difficult to probe at the LHC. Note that the $H_5^{\pm\pm}$ can also be produced associated with single-charged component (H_5^\pm) of the fiveplet. However, the discussion on the phenomenology of H_5^{\pm} depends on the details of the parameter space. In this work, we focus on the analysis of the signature from $H_5^{\pm\pm}$ with the dependence only on two parameters m_5 and s_H , which can thus be easily generalized to any other situation with doubly-charged scalar particles.

2. The decay of
$$H_5^{\pm\pm} \to W^{\pm}W^{\pm}$$

In the GM model, no lepton number violation interaction is introduced. Hence, if the fiveplet is lighter than the scalar triplet (which contains a single-charged component H_3^{\pm}), $H_5^{\pm\pm}$ has only one decay channel $H_5^{\pm\pm} \to W^{\pm}W^{\pm}$. Although, the branching ratio will never change, the decay width highly relies on the mass m_5 and the couplings between $H_5^{\pm\pm}$ and W^{\pm} which is proportional to s_H [82]. In particular, when the mass m_5 is below the threshold $2m_W$, the decay can only happen through at least one off-shell W. On the other hand, current measurements from direct searches of heavy particles and from the Higgs signal strength give rise to strong constraints on s_H which indicates the contribution of the $SU(2)_L \times SU(2)_R$ triplet vev to the total vev. Both situations will greatly suppress the decay width of $H_5^{\pm\pm}$ in the low- m_5 and low- s_H region.

Analytically, the decay width of $H_5^{\pm\pm} \to W^{\pm}W^{\pm}$ including the off-shell effect is given by [83, 84]

$$\Gamma(H_5^{\pm\pm} \to W^{\pm}W^{\pm}) = \frac{1}{\pi^2} \int_0^{m_{H_5}^2} dQ_1^2 \int_0^{(m_{H_5} - Q_1)^2} dQ_2^2
\times \frac{Q_1^2 \Gamma_{W^{\pm}} / M_{W^{\pm}}}{(Q_1^2 - M_{W^{\pm}}^2)^2 + M_{W^{\pm}}^2 \Gamma_{W^{\pm}}^2} \frac{Q_2^2 \Gamma_{W^{\pm}} / M_{W^{\pm}}}{(Q_2^2 - M_{W^{\pm}}^2)^2 + M_{W^{\pm}}^2 \Gamma_{W^{\pm}}^2} \Gamma_5^{H_5^{\pm\pm}W^{\pm}W^{\pm}} (Q_1^2, Q_2^2), \quad (27)$$

where $\Gamma_{W^{\pm}}$ is the width of W boson and Q_i^2 is the square of the four-momentum of W boson. $\Gamma^{H_5^{\pm\pm}W^{\pm}W^{\pm}}(Q_1^2,Q_2^2)$ is given by

$$\Gamma^{H_5^{\pm\pm}W^{\pm}W^{\pm}}(Q_1^2, Q_2^2) = S_V \frac{|g_{H_5^{\pm\pm}W^{\pm}W^{\pm}}|^2 m_{H_5^{\pm\pm}}^3}{64\pi Q_1^2 Q_2^2} \left[1 - 2k_1 - 2k_2 + 10k_1 k_2 + k_1^2 + k_2^2\right] \lambda^{1/2}(k_1, k_2),$$
(28)

where $S_V = 1/2$ is the symmetry factor, $k_i = Q_i^2/m_5^2$ and $\lambda(x, y)$ is the kinematic function given by

$$\lambda(x,y) = (1 - x - y)^2 - 4xy. \tag{29}$$

The coupling involved in this decay is given by

$$g_{H_{\varepsilon}^{\pm\pm}W^{\mp}W^{\mp}} = \sqrt{2}g^2vs_H. \tag{30}$$

Hence, the decay width is suppressed by mainly two factors. First, it will be suppressed by the tails of at least one of the Breit-Wigner resonants factors in Eq. (27) when $m_5 < 2m_W$.

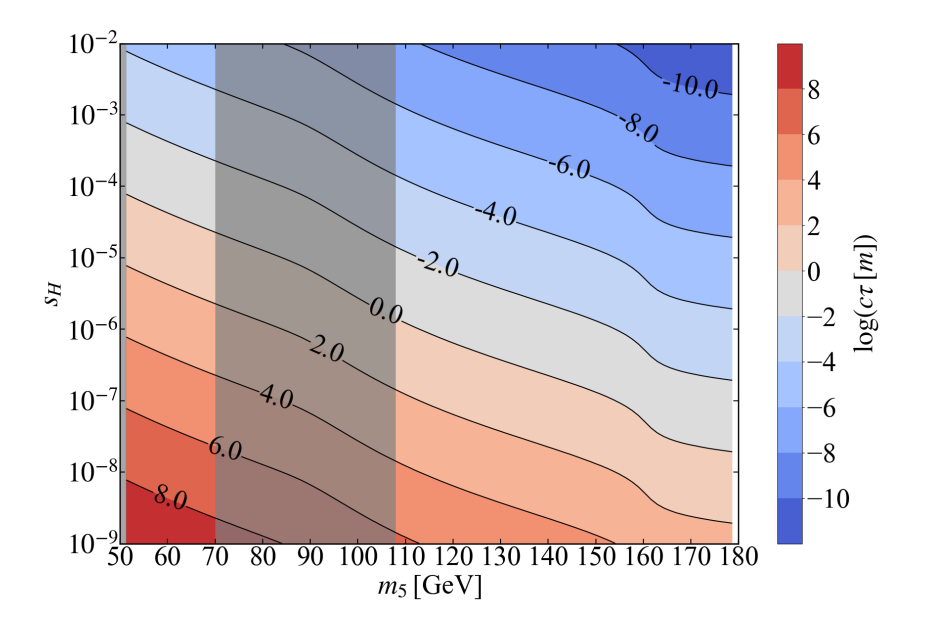


FIG. 3. The proper decay length $(c\tau)$ of $H_5^{\pm\pm}$ in the m_5 - s_H plane. The gray areas indicate the parameter regions that are excluded by diphoton searches in low- m_5 benchmark.

The width will further be suppressed by s_H through $g_{H_5^{\pm\pm}W^{\mp}W^{\mp}}$ in Eq. (28). It is thus nature to expect that the decay width will be suppressed strongly in low- m_5 and low- s_H region such that $H_5^{\pm\pm}$ will travel some distance before it decays into SM particles which significantly alters the signatures at the LHC.

The proper decay length of $H_5^{\pm\pm}$ in the m_5 - s_H plane is shown in Fig. 3. It is clear that the decay length $c\tau$ increase with the decrease of both m_5 and s_H . It shows clearly the threshold effects around $m_5 \sim 160\,\mathrm{GeV}$ as well. In the lower left corner, $c\tau$ can easily reach several meters or even hundred/thousand meters which is the parameter region that can be covered by LLP searches at the LHC as well as in the far detectors. As we have discussed above, the long-lived nature of $H_5^{\pm\pm}$ in this parameter space invalidates most of the current searches of doubly-charged scalar. The most relevant search, which still depends on the details of the parameter space, comes from the diphoton resonant searches. The neutral component of the fiveplet H_5^0 will have a dominant decay channel $H_5^0 \to \gamma\gamma$ in the mass region of interests, which is not suppressed by the phase space [85]. Such channel has already been covered at the LHC from both ATLAS [86, 87] and CMS [88, 89]. We recast the results in the low- m_5 benchmark and show the excluded region by gray area in Fig. 3. The region with $70\,\mathrm{GeV} \lesssim m_5 \lesssim 108\,\mathrm{GeV}$ and a tiny region with $m_5 \sim 50\,\mathrm{GeV}$ of the low- m_5

benchmark are excluded by diphoton searches. Note that the decay width of $H_5^0 \to \gamma \gamma$ has contributions that do not depend on s_H , the diphoton searches can cover the relevant region extending the whole range of s_H . However, this depends on the details of the parameter space. In particular, different contributions i.e. from W^{\pm} loop and H_3^{\pm} loop, can cancel with each other to suppressed the decay ratio such that the diphoton searches no longer have sensitivity.

III. SEARCHING FOR THE LONG-LIVED $H_5^{\pm\pm}$ AT THE LHC AND IN FAR DETECTORS

As discussed in previous section, in specific parameter region of m_5 - s_H plane, $H_5^{\pm\pm}$ becomes long-lived which significantly alters the signatures at the LHC. In this section, we will discuss the signatures of long-lived $H_5^{\pm\pm}$ at the ATLAS/CMS detectors as well as the detectors located far away from the interaction point (IP). In the first case, we will focus on the scenarios where $H_5^{\pm\pm}$ travels some distance before it decays within the detectors (in different layers) or $H_5^{\pm\pm}$ travels outside the detectors but still leaves signal through its charged track. Finally, we will discuss the case where $H_5^{\pm\pm}$ travels a long distance and leaves signals in various far detectors.

The general-purpose detectors, although are different in details, share similar structures as shown in Fig. 4. From inside out, it consists of inner tracking detector (ID), electromagnetic calorimeter (ECal), hadronic calorimeter (HCal) and muon system (MS) [90]. The ID, ECal and HCal will be covered by strong magnetic field. For long-lived $H_5^{\pm\pm}$, we consider detecting the displaced objects within either ID or MS. The analysis of displaced calorimeter deposits in ECal and HCal [90] is not considered in this work as it requires dedicated calorimeter simulation and the design of a suitable trigger system, which are beyond the scope of this study. Further, when the $H_5^{\pm\pm}$ travels outside the detector, it will be treated as heavy stable charged particle (HSCP). In particular, the trajectory of $H_5^{\pm\pm}$ will have smaller radius within the magnetic field⁴, as it is doubly charged, which is included in the consideration of HSCP analysis. The far detectors are extensions of the ATLAS/CMS/LHCb/ALICE detectors. These far detectors can also probe the HSCP scenario when the LLP decays within the corresponding detector volume.

 $^{^4}$ The trajectory of charged particles in magnetic field is given in Appendix A.

	Electrons	Muons
Transverse momentum	$p_T > 42 \text{ GeV}$	$p_T > 40 \text{ GeV}$
	$ \eta < 1.44$	
Pseudorapidity (η)	or	$ \eta < 2.4$
	$1.56 < \eta < 2.4$	
Isolation cone	$\Delta R < 0.3$	$\Delta R < 0.4$
Isolation variable	$\frac{p_T^{\rm iso}}{p_T} < 0.035 \; (\eta < 1.44)$	
with		$\left \frac{p_T^{\text{iso}}}{p_T} < 0.15 \; (\eta < 2.4) \right $
its $ \eta $ coverage	$\left \frac{p_T^{\text{iso}}}{p_T} < 0.065 \right (1.56 < \eta < 2.4)$	

TABLE II. Summary of the basic selections imposed on the candidate electrons and muons.

In current studies, we focus on the pair production of $H_5^{\pm\pm}$ via the process $p\,p\to H_5^{++}H_5^{--}$ at the LHC with $\sqrt{s}=14\,\text{TeV}$ and $\mathcal{L}=300/3000\,\text{fb}^{-1}$. For a long-lived doubly charged particle in the final state, after proper event selections, the relevant background can be reduced to a negligible level. We thus assume that the signal region we considered is background-free.

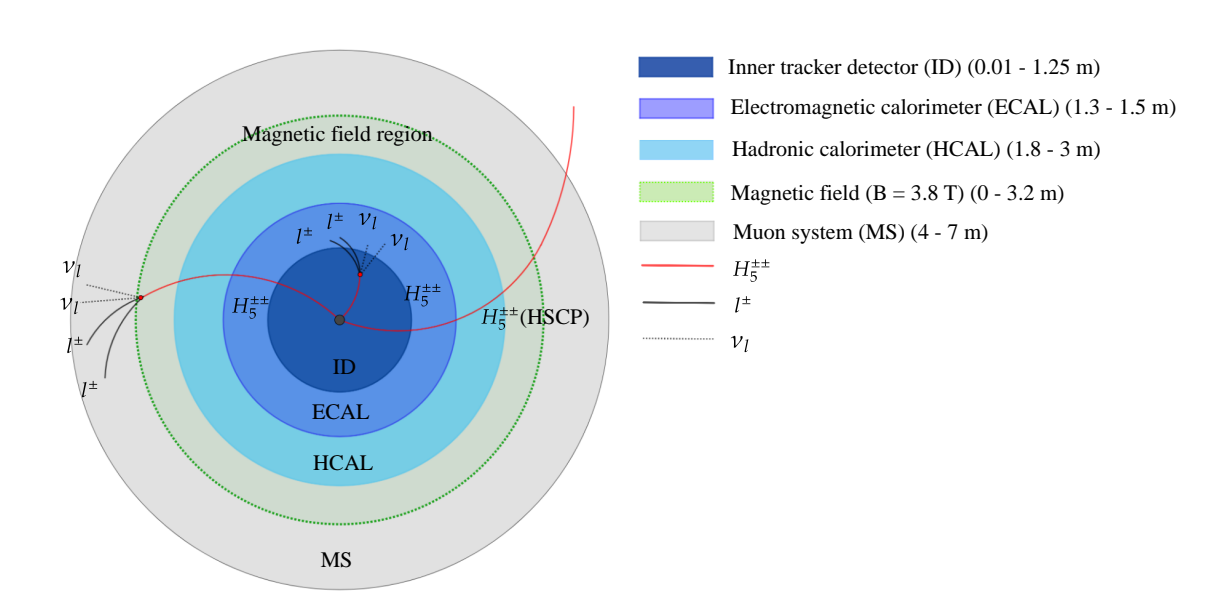


FIG. 4. Several main subsystems of the generic detectors (ATLAS/CMS) at the LHC [90].

A. $H_5^{\pm\pm}$ decays within the inner tracking detector

We first focus on the long-lived $H_5^{\pm\pm}$ decays within the inner tracker system. Here, the leptonic decay modes of $H_5^{\pm\pm}$ are considered: $H_5^{\pm\pm} \to \ell^{\pm} \nu_{\ell} \ell^{\pm} \nu_{\ell}$ where $\ell=e,\mu,$ as the signature of a displaced vertex with same-sign charged leptons can largely reduce possible background events. The signal events are generated by MadGraph5 [75] and then passed to Pythia8 [91] for showering and hadronization. At the generator level, we applied the following basic cuts for the final state charged leptons: $p_T^\ell > 10\,\mathrm{GeV}, \, |\eta_\ell| < 2.5$ and $\Delta R_{\ell\ell} > 0.4$. To simulate the detector effects, we use the simplified-fast simulation (SFS) framework [92] embedded in MadAnalysis5 [93]. This analysis utilized the CMS-EXO-16-022 template SFS card [92], and the effect of the magnetic field on particle trajectory deflection within the SFS framework was determined for the transverse impact parameter, $d_{0,\ell}$. The leptons (electron or muon) from the $H_5^{\pm\pm}$ decay should satisfy the basic event selections listed in Tab. II [59], which require a energetic (minimum value for p_T) isolated charged leptons (requirement on p_T^{iso}) that can be covered by the corresponding detector layers (range of η). Here p_T^{iso} is defined as the scalar sum of the transverse momentum of all reconstructed objects lying within a cone of a specified size $\Delta R < 0.3$ and is centered around the momentum of the leptons. The recasting analysis [59] in the Public Analysis Database (PAD) [94–97] are then adapted for our purpose for the long-lived $H_5^{\pm\pm}$ decaying within the ID.

The following event selections are applied further in order to single out the signal events:

- 1. At least one pair of charged leptons with the same charge,
- 2. $0.2 < |d_{0,\ell}| < 100 \text{ mm},$
- 3. $\rho_{\ell} < 10 \text{ cm} \text{ and } z_{\ell} < 30 \text{ cm},$
- 4. $\Delta R_{\ell^{\pm}\ell'^{\pm}} < 1.5$,
- 5. $E_T > 20 \text{ GeV}$,
- 6. Veto $0.7 < \Delta \phi_{\ell^{\pm}\ell'^{\pm}}^{miss} < 2.5$ with $\Delta \phi_{\ell^{\pm}\ell'^{\pm}}^{miss} \equiv |\Delta \phi(\vec{p}_T^{miss}, \vec{p}_T^{\ell^{\pm}\ell'^{\pm}})|$,

where $\ell = e, \mu$ and ρ_{ℓ} , z_{ℓ} are the transverse and longitudinal distance, with respect to the IP, of the lepton production vertex, defined as the intersection point of the tracks from

the same-sign charged leptons. $\Delta R_{\ell^{\pm}\ell'^{\pm}}$ is the distance in η - ϕ plane between two samesign leptons, \not{E}_T is the transverse missing energy, $\Delta \phi_{\ell^{\pm}\ell'^{\pm}}^{miss}$ represents the azimuthal angular separation between the missing transverse momentum (\vec{p}_T^{miss}) and the transverse momentum of a pair of same-sign charged leptons $(\vec{p}_T^{\ell^{\pm}\ell'^{\pm}})$, $d_{0,\ell}$ is the transverse impact parameter for the corresponding charged lepton ℓ as shown in Fig. 5 for $|d_{0,\ell}|$ in $H_5^{\pm\pm} \to \ell^{\pm}\nu_{\ell}\ell^{\pm}\nu_{\ell}$ case where both the $H_5^{\pm\pm}$ and the charged leptons will be bended by the strong magnetic field which is considered in the analysis according to Appendix A.

Pair production of leptonic decay $H_5^{\pm\pm}$ provides at least one pair of same-sign charged leptons. In order to suppress the background from multi-gauge boson productions, we observed that the decay products of $H_5^{\pm\pm}$ tend to be collinear, resulting in a smaller separation between the two same-sign charged leptons. On the other hand, pair of $H_5^{\pm\pm}$ are produced back-to-back in the transverse plane, the transverse momentum of the pair of two same-sign charged leptons, $\vec{p}_T^{\ell^{\pm}\ell'^{\pm}}$, is close to either the same or opposite direction of \vec{p}_T^{miss} . Therefore, we require $\Delta R_{\ell^{\pm}\ell'^{\pm}} < 1.5$ for the pair of same-sign charged leptons and veto $0.7 < \Delta \phi_{\ell^{\pm}\ell'^{\pm}}^{\text{miss}} < 2.5$ to suppress the multi-gauge boson backgrounds. Further, the long-lived nature of $H_5^{\pm\pm}$ and

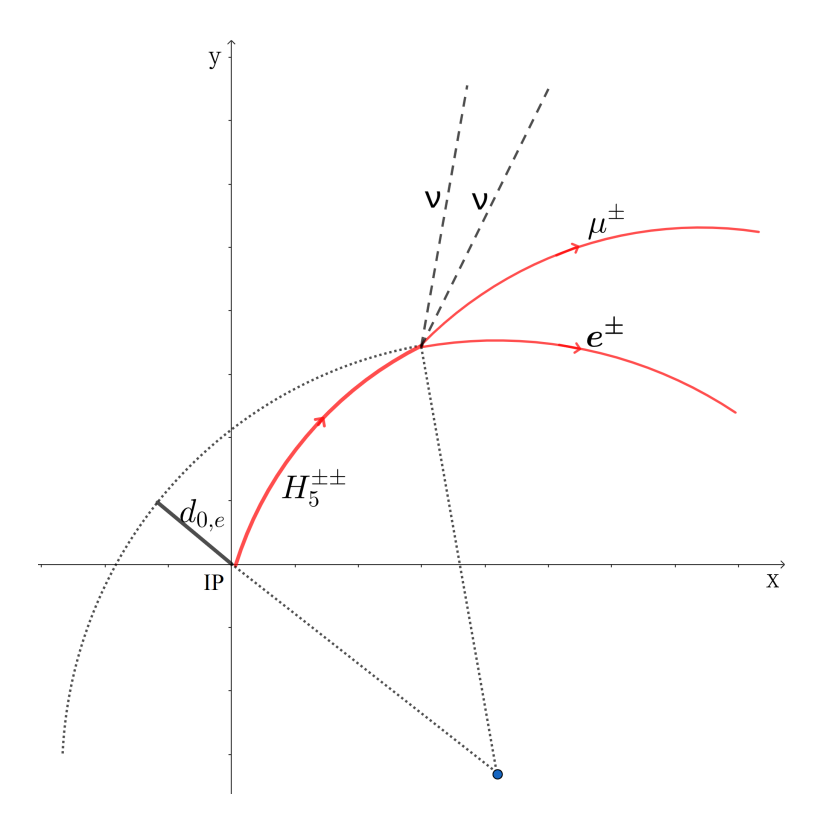


FIG. 5. Definition of the transverse impact parameter $d_{0,\ell}$ [59] in the tracker system.

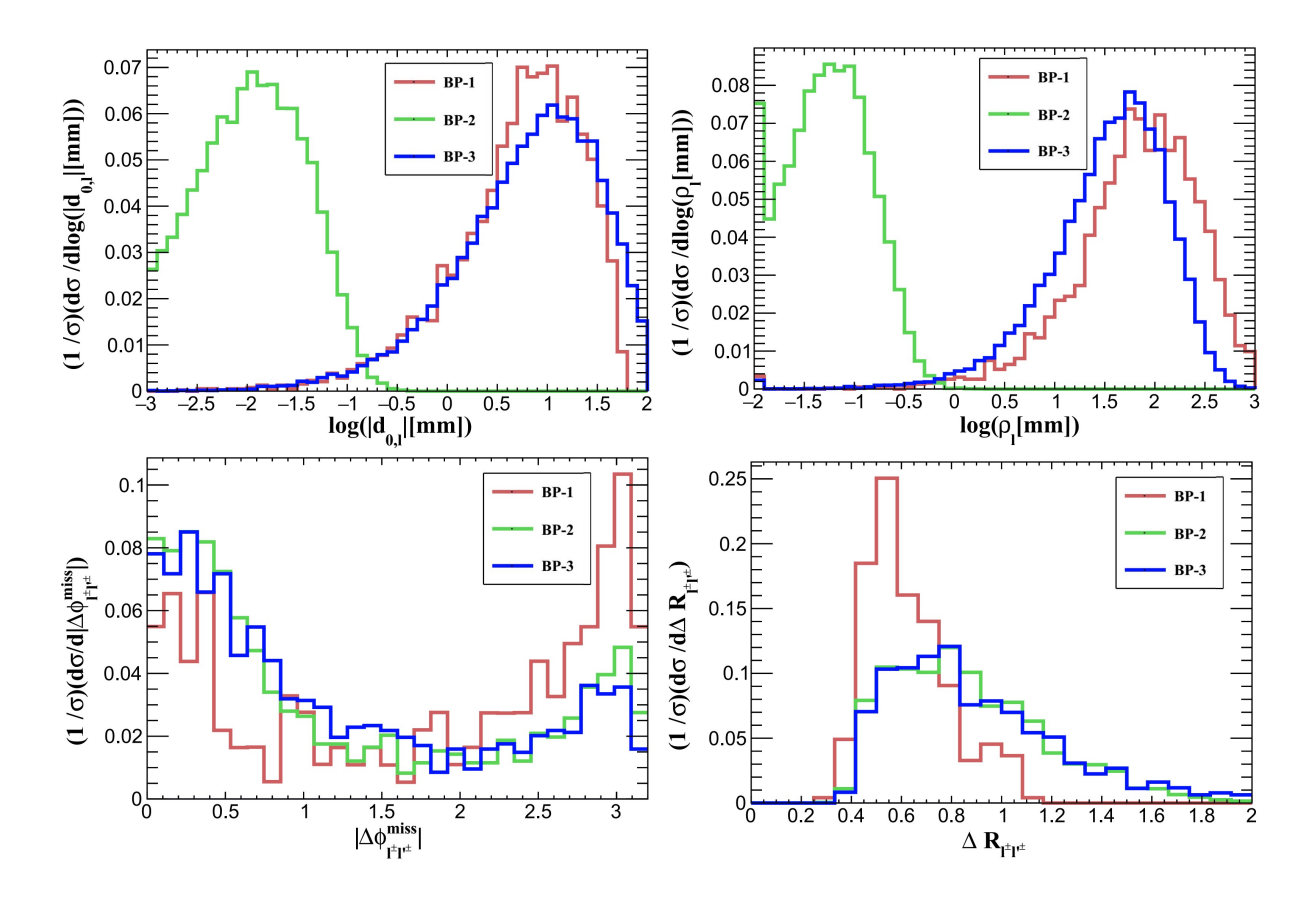


FIG. 6. $d_{0,\ell}$, ρ_{ℓ} , $|\Delta\phi_{\ell^{\pm}\ell'\pm}^{\rm miss}|$ and $\Delta R_{\ell^{\pm}\ell'\pm}$ distributions for $H_5^{\pm\pm}$ leptonic decay within ID for three benchmarks: BP-1 (red) $m_5 = 70\,{\rm GeV}, s_H = 5\times 10^{-5}$; BP-2 (green) $m_5 = 130\,{\rm GeV}, s_H = 5\times 10^{-5}$ and BP-3 (blue) $m_5 = 130\,{\rm GeV}, s_H = 8\times 10^{-7}$.

Cut flow in σ [fb]	BP-1	BP-2	BP-3
Generator	8.221	3.927	3.927
Same-sign lepton pair ≥ 1	0.253	0.383	0.381
$0.2 < d_{0,\ell} < 100 \text{ mm}$	0.251	4.03×10^{-2}	0.356
$\rho_{\ell} < 10 \text{ cm}, z_{\ell} < 30 \text{ cm}$	2.40×10^{-2}	3.82×10^{-2}	3.47×10^{-2}
$\Delta R_{\ell^{\pm}\ell'^{\pm}} < 1.5$	2.31×10^{-2}	3.70×10^{-2}	3.31×10^{-2}
$E_T > 20 \text{ GeV}$	2.09×10^{-2}	3.34×10^{-2}	3.09×10^{-2}
$\Delta\phi$ veto	1.81×10^{-2}	3.12×10^{-2}	2.92×10^{-2}

TABLE III. The cut-flow table for $H_5^{\pm\pm}$ leptonic decay within ID for the three benchmark points. The details of each selection are listed in the main text.

the requirement of the decay within ID provide that $\rho_{\ell} < 10 \,\mathrm{cm}$ and $z_{\ell} < 30 \,\mathrm{cm}$ which are adapted from [59], and also $0.2 < |d_{0,\ell}| < 100 \,\mathrm{mm}$. The $d_{0,\ell}$, ρ_{ℓ} , $\Delta R_{\ell^{\pm}\ell'^{\pm}}$ and $\Delta \phi_{\ell^{\pm}\ell'^{\pm}}^{\mathrm{miss}}$ distributions are shown in Fig. 6 for three benchmarks:

- BP-1: $m_5 = 70 \text{ GeV}, s_H = 5 \times 10^{-5},$
- BP-2: $m_5 = 130 \text{ GeV}, s_H = 5 \times 10^{-5},$
- BP-3: $m_5 = 130 \text{ GeV}, s_H = 8 \times 10^{-7}.$

Note that, the s_H for BP-3 is chosen such that it has roughly the same $c\tau$ as BP-1. BP-2 has smaller $c\tau$ than BP-1 and BP-3. Hence, BP-2 has much smaller $d_{0,\ell}$ and ρ_{ℓ} than BP-1 and BP-3 as can be seen from Fig. 6. On the other hand, other kinematic distributions are not sensitive to the $c\tau$ and depends only on the mass of the $H_5^{\pm\pm}$. The cut-flow table for the cross section of above three benchmark points are shown in Tab. III. With these cuts, especially the requirement of a same-sign lepton pair, the range for ρ_{ℓ} and $d_{0,\ell}$, the background is assumed to be negligible.

The number of signal event is then obtained as $N_S = \epsilon \times \sigma \times \mathcal{L}$ where ϵ is the selection efficiency calculated for different m_5 and s_H , σ is the signal cross section without any cut. In this study, we assume $\mathcal{L} = 300/3000 \,\mathrm{fb}^{-1}$. For the background-free case, $N_S = 3$ defines the 95% confidence level (CL.) exclusion limit. We then extend the same search strategies over a wide range of m_5 values and the 95% exclusion regions in m_5 - $c\tau$ plane as well as m_5 - s_H plane are shown in the blue area of Fig. 8. One can see the searches from inner tracker can cover the $c\tau$ from 10^{-4} m to about 1 m. The coverage becomes weak at lower mass, as the efficiency drops due to a fixed basic cuts on the final states.

B. $H_5^{\pm\pm}$ decays within the muon system

If the lifetime of $H_5^{\pm\pm}$ is much longer, it may travel through the tracker and calorimeters and decay within the muon system. In particular, in the following analysis, we consider the case where the decay happens in the CMS endcap muon detectors (EMDs) where the cathode strip chambers (CSCs) are installed. This analysis uses the CMS-CSCCluster template card [98] in Delphes to simulate the efficiency of detector reconstruction clusters and the effect of the magnetic field on the charged trajectories of LLPs within the detector. The

detailed configurations of the detectors can be found in [60, 99, 100]. The analysis follows the CMS searches for LLPs decaying in the EMDs [60] and the recasting analysis which tabulates the efficiency of CSCs of the CMS experiments [101] ⁵. Using the CSCs for LLP searches can efficiently reduce the background to a sufficiently low level thanks to a large amount of absorber material in front of the EMD acting as a shield. Further, the CSCs as sampling calorimeter are more sensitive to the LLP energy rather than its mass. It hence provides equally sensitivity to all LLP masses considered here.

We consider all possible decay channels of $H_5^{\pm\pm}$ in this case: leptonic $(H_5^{\pm\pm} \to \ell^{\pm}\nu_{\ell}\ell^{\pm}\nu_{\ell})$, hadronic $(H_5^{\pm\pm} \to jjjj)$ and semi-leptonic $(H_5^{\pm\pm} \to \ell^{\pm}\nu_{\ell}jj)$. Note that the muon can penetrate the shield easily, for the above channels, we thus require the signal signature with at least a pair of same charged muons or a CSC cluster from one $H_5^{\pm\pm}$ in order to suppress relevant background events. At the generator level, we required $p_T^{\ell} > 10 \,\mathrm{GeV}$, $|\eta_\ell|$ < 2.5 and $\Delta R_{\ell\ell}$ > 0.4 for leptons, and p_T^j > 20 GeV, $|\eta_j|$ < 5.0, ΔR_{jj} > 0.4 and $\Delta R_{j\ell} > 0.4$ for jets. In this case, $H_5^{\pm\pm}$ is assumed to decay into jets or leptons within the muon system, and its decay products will leave signals in the CSC detectors. The response of the CSC detector is simulated with relevant modules in delphes using the tabulated efficiency extracted from the CMS results [60]. After reconstruction, the final states contain muons and/or CSC cluster which is the group of the signals from different layers/components of CSCs. The final state muon is reconstructed in the usual way, but is required to have $1.5 < |\eta| < 2.4$ within the coverage of CSC detectors. The muon should further satisfy the isolation requirements: $\frac{\sum_i p_T^{\text{particle}_i}}{p_T^{\mu}} \leq 0.25$, where the summation is over all particles inside the isolation cone $\Delta R = \sqrt{(\Delta \eta)^2 + (\Delta \phi)^2} \leq 0.5$ with $p_T^{\text{particle}} > 0.5$ GeV, and p_T^{μ} is the transverse momentum of the muon.

The reconstructed CSC cluster is required to satisfy the following requirements:

- Containing at least 50 hits in the CSC detectors,
- CSC cluster time between -5 ns and 12.5 ns to reject clusters produced by pileup,
- All clusters within a distance of $\Delta R = \sqrt{(\Delta \eta)^2 + (\Delta \phi)^2} < 0.4$ from a muon are removed to ensure that the *CSC cluster* is not associated with muons having $p_T \geq 10$ GeV, and to prevent the cluster from being generated by muon bremsstrahlung [102].

⁵ The tabulated efficiency of CSC is available in relevant modules in Delphes, see https://github.com/delphes/delphes/pull/103.

Type	e^{\pm}	$e^{\pm}e^{\pm}$	jj	jjjj	jje^{\pm}
Efficiency for $m_5 = 70 \text{GeV}$	7.6%	8.2%	2.9%	3.2%	8.0%
Efficiency for $m_5 = 130 \text{GeV}$	10.7%	11.7%	4.0%	5.1%	11.2%

TABLE IV. The reconstruction efficiency of CSC cluster induced from different decay products of $H_5^{\pm\pm}$ for two mass benchmarks with $m_5 = 70\,\text{GeV}$ and $m_5 = 130\,\text{GeV}$.

In the current case, the CSC cluster is induced either by the electron or the jet from the $H_5^{\pm\pm}$ decay. However, any such decay products from the same $H_5^{\pm\pm}$ (and thus traveling in similar directions) will result in at most one CSC cluster, even if both hit the same groups of CSC detectors. For CSC cluster induced by various combinations of the electron and/or jet decay products from $H_5^{\pm\pm}$, the reconstruction efficiencies are listed in Tab. IV for two mass benchmarks, $m_5 = 70$ GeV and 130 GeV. It is evident that with higher energy from $H_5^{\pm\pm}$ due to a heavier mass, the efficiency increases.

The analysis is classified into four channels according to the number of CSC cluster N_C and the number of same-sign muon pair N_{μ}^{SS} :

- 1. $N_C=2, N_{\mu}^{SS}=0$, where both $H_5^{\pm\pm}$ decay into electrons or jets and are all reconstructed as CSC cluster.
- 2. $N_C = 1, N_{\mu}^{SS} = 0$, where only one of $H_5^{\pm\pm}$ s is reconstructed as *CSC cluster* and the other one escapes from the detector.
- 3. $N_C = 1, N_{\mu}^{SS} = 1$, where one of $H_5^{\pm\pm}$ s is reconstructed as *CSC cluster* and the other decays into a pair of muons.
- 4. $N_C = 0, N_{\mu}^{SS} = 1$, where one $H_5^{\pm\pm}$ is reconstructed through its muonic decay channel, and the other one escapes from the detector.
- 5. $N_C = 0, N_{\mu}^{SS} = 2$ (one positive and one negative muon pair), where both $H_5^{\pm\pm}$ decay into a pair of muons.

The signal cross sections of these five channels for two benchmark points $m_5 = 70$ GeV with $s_H = 3.2 \times 10^{-5}$ and $m_5 = 130$ GeV with $s_H = 3.8 \times 10^{-7}$ are listed in Tab. V, where the requirement that $H_5^{\pm\pm}$ should decay within the CSC detector is also included. As mentioned

- [a-]	$m_5 = 70 \text{ GeV}$	$m_5 = 130 \text{ GeV}$
σ [fb]	$s_H = 3.2 \times 10^{-5}$	$s_H = 3.8 \times 10^{-7}$
$N_C = 2, N_\mu^{SS} = 0$	1.80×10^{-3}	6.44×10^{-3}
$N_C = 1, N_\mu^{SS} = 0$	2.71×10^{-2}	1.00×10^{-1}
$N_C = 1, N_\mu^{SS} = 1$	6.36×10^{-4}	7.48×10^{-3}
$N_C = 0, N_\mu^{SS} = 1$	7.99×10^{-4}	9.56×10^{-2}
$N_C = 0, N_\mu^{SS} = 2$	2.32×10^{-4}	1.53×10^{-2}
Total	3.10×10^{-2}	2.24×10^{-1}

TABLE V. The cross section for $H_5^{\pm\pm}$ decaying in CSC detector for four different channels of two benchmark points: $m_5 = 70$ GeV with $s_H = 3.2 \times 10^{-5}$ and $m_5 = 130$ GeV with $s_H = 3.8 \times 10^{-7}$.

above, we do not include the case where one $H_5^{\pm\pm}$ only produces one muon together with other particles. However, we have also checked the event rate from such signature, which only provides several percent increase in the total rate. We then extend the same search strategies over a wide range of m_5 values and the 95% exclusion regions in m_5 - $c\tau$ plane as well as m_5 - s_H plane are shown in the pink area of Fig. 8. Notably, the searches with CSC detector of the muon system can cover the $c\tau$ of $H_5^{\pm\pm}$ from below meter to about 10-100 meters almost independent of the $H_5^{\pm\pm}$ mass.

C. $H_5^{\pm\pm}$ as a heavy stable charged particle

If the $H_5^{\pm\pm}$ has even longer lifetime, it can travel through the whole detector before its decay, there is no explicit signal except the charged tracks in the detector, rendering it as heavy stable charged particle (HSCP). Without a dedicated search strategy, there is a risk of misidentification or complete oversight of HSCPs, as the particle identification algorithm in hadron collider experiments is often tailored to signature characteristics of SM particles. Both ATLAS and CMS have performed detailed analysis about the HSCP with full detector simulations which put strong constraints on the production cross section of such particles [103, 104].

However, in order to apply the relevant results on GM model, one needs dedicated simulation of the detector response for the doubly charged $H_5^{\pm\pm}$ which is beyond the scope of

current work. The CMS Collaboration proposed a "fast technique" [105] to simulate the response of the detector to HSCPs which is embedded in an efficiency table as function of p_T , η and β of the charged tracks. Nevertheless, this efficiency table is currently provided only for singly charged HSCP. For doubly charged HSCP, the energy deposition will change dramatically which alters significantly the detector efficiency. On the other hand, doubly charged HSCP, with the same momentum, will have smaller tracking radius compared to singly charged HSCP. Combining all of these factors, it is not reliable to use this efficiency table for our case. Hence, for the current case, we do not estimate the prospects of detecting $H_5^{\pm\pm}$ as a HSCP , as this would require a detailed simulation of the detector response. Instead, we simply apply the previous constraints on the production cross section from the 7/8 TeV analysis [106]. The analysis performed in [106] for multiple charged HSCPs utilizes the energy deposition information in the detector and the time-of-flight (TOF) measurement from the muon system. The multiply charged particles will produce greater ionization in the detector compared to singly charged particles. The β inferred from the TOF measurement for a relatively heavy particle will be smaller than that of SM particles. In order to apply the constraint in our case, for each mass of $H_5^{\pm\pm}$ and its $c\tau$, we calculate the cross section of $H_5^{\pm\pm}$ production that can flight out of the detector. With varying η , the minimum travel distance required to traverse the entire detector will differ slightly. Here, we follow the conservative estimation of such threshold from [105] requiring

$$L \ge \begin{cases} 9.0 \,\mathrm{m}, & 0.0 \le |\eta| \le 0.8, \\ 10.0 \,\mathrm{m}, & 0.8 \le |\eta| \le 1.1, \\ 11.0 \,\mathrm{m}, & 1.1 \le |\eta|. \end{cases}$$
 (31)

The traveling distance can be estimated statistically event by event according to the momentum of $H_5^{\pm\pm}$ and its $c\tau$. In the lab frame, the probability of $H_5^{\pm\pm}$ can travel longer than some threshold L is given by $\exp(-L/\gamma\beta\tau)$. The production cross section $H_5^{\pm\pm}$ is scaled by such probability and we ignore the case where $H_5^{\pm\pm}$ decay before travelling above the threshold distance which is already covered by the analysis in the above sections. The cross section is then compared with the upper limit provided by the CMS [106] with $\sqrt{s} = 7/8$ TeV. The results are shown in yellow area ($\sqrt{s} = 7$ TeV) and orange area ($\sqrt{s} = 8$ TeV) of Fig. 8 with coverage only above $m_5 > 100$ GeV. The region above (below) corresponding $c\tau$ (s_H) can all be excluded. The exclusion line in $c\tau$ is well aligned with the size of the detector. Therefore,

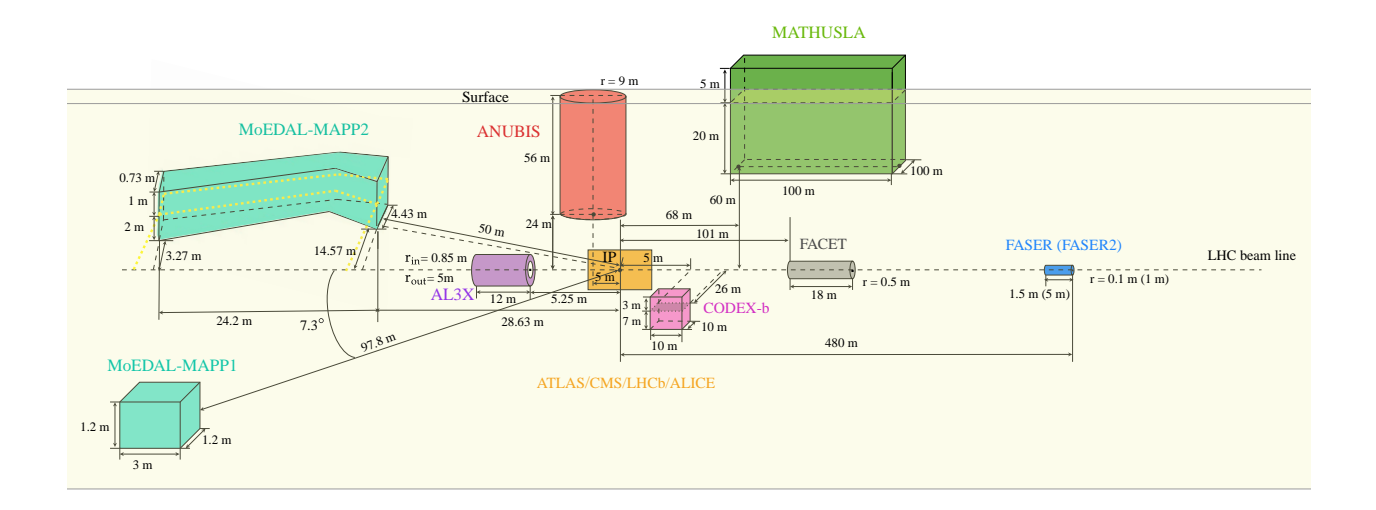


FIG. 7. The positions of far detectors relative to ATLAS/CMS/LHCb/ALICE detectors including ANUBIS, MATHUSLA, FACET, FASER, COEDX-b, MoEDAL-MAPP and AL3X. To better illustrate the position and size of the detectors, the picture is not drawn to scale, however, the marked values reflect the actual dimensions.

we expect that even with higher energy and higher luminosity, the exclusion will not change too much.

D. $H_5^{\pm\pm}$ decays in far detectors

Similar to the case discussed in Section III C, $H_5^{\pm\pm}$ can traverse the entire detectors with a sufficiently long lifetime. In addition to treating it as a HSCP, various detectors located farther from the interaction point (IP) can be used to identify signals from such LLPs. These detectors include ANUBIS [61], MATHUSLA [62], FACET [63], FASER/FASER2 [64], CODEX-b [65], MoEDAL-MAPP [66] and AL3X [67]. The locations of these detectors relative to the ATLAS/CMS/LHCb/ALICE detectors are shown in Fig. 7, where we indicate the distance to the IP and the geometric size of each detector.

- MAssive Timing Hodoscope for Ultra-Stable neutraL pArticles, MATHUSLA [62, 107] is a box-shaped detector with dimensions of 100 m × 100 m × 25 m for detecting LLPs. It is located about 70 m away from CMS IP, with approximately 20 m of decay volume below surface and 5 m of decay volume above surface.
- AN Underground Belayed In-Shaft, ANUBIS [61, 108, 109] is a proposed cylindrical

detector that uses the ATLAS installation shafts with a diameter of 18 m and a length of 56 m for experimentation. The detector is placed 24 m above the ATLAS IP with 5 m offset.

- Forward-Aperture CMS ExTension, FACET [63] is a cylindrical detector with 0.5 m radius and 18 m length located 119 m away from the CMS IP along the longitudinal direction.
- The Forward Search Experiment, FASER [64, 110] is designed to search light particles with extremely weak interactions. The detector is located 480 m away from the ATLAS IP along the longitudinal direction. FASER detector, which is already installed, is a cylindrical detector with 0.1 m radius and 1.5 m length. The future upgrade FASER2 will extend its radius to 1 m and length to 5 m.
- COmpact Detector for EXotics at LHCb, CODEX-b [65, 111] is a $10 \times 10 \times 10 \,\mathrm{m}^3$ cube detector located 25 m away from the LHCb IP which covers the range of $x \in [26, 36] \,\mathrm{m}$, $y \in [-7, 3] \,\mathrm{m}$ and $z \in [5, 15] \,\mathrm{m}$, where the z-axis is along the beamline at the IP, the y-axis is perpendicular to the ground.
- MoEDAL's Apparatus for Penetrating Particles, MAPP [66, 112, 113] is a detector designed for LLPs in the MoEDAL [114–116] experiment frame. Phase 1 of MAPP(MAPP1) with 30 fb⁻¹ is located in the UA83 tunnel about 97.8 m from the LHCb IP, with a 7.3° angle relative to the beam direction. Its dimension is 1.2m×1.2m×3m. Phase 2 of MAPP(MAPP2) with 300 fb⁻¹ is a detector planned to be built in the UGC1 tube approximately 50m from the LHCb IP. It is composed of two polyhedra.
- A Laboratory for Long-Lived eXotics, AL3X [67, 117] is a cylindrical detector located in the LHC-ALICE/L3 cave, 5.25 m from the collision site. It has a length of 12 m and an inner and outer radius of 0.85 and 5 m, respectively.

For these far detectors, we assume that whenever the LLP decays within the detector volume, it can be detected. To evaluate the sensitivity of the far detectors, the Display Decay Counter (DDC) [110] is utilized to estimate the probability for a given LLP decaying within the corresponding detectors. In particular, along its trajectory, the probability that

the particle decays traveling a distance between ℓ_1 and ℓ_2 in the lab frame is given by

$$\mathcal{P}(\ell_1, \ell_2) = \exp\left[-\frac{\ell_1}{\gamma \beta \tau}\right] - \exp\left[-\frac{\ell_2}{\gamma \beta \tau}\right]$$
 (32)

where β is the velocity of the particle, $\gamma = (1 - \beta^2)^{-1/2}$, τ is the proper lifetime of the particle. For a given event containing the LLP, ℓ_1 and ℓ_2 can be determined by the direction of the LLP and the boundaries of the corresponding detector.

Considering that the signal from the IP has strong directional information and that the thick rock coverage in between will block all SM particles, the analysis can be considered to be background-free. The coverages for various far detectors in both m_5 - $c\tau$ and m_5 - s_H planes are shown in Fig. 8. The region within the corresponding lines is excluded at 95% CL. with $\mathcal{L} = 300/3000\,\mathrm{fb^{-1}}$ for ANUBIS, MATHUSLA, FACET and FASER/FASER2, $\mathcal{L} =$ $30/300\,\mathrm{fb^{-1}}$ for CODEX-b and MoEDAL-MAPP, $\mathcal{L}=100/250\,\mathrm{fb^{-1}}$ for AL3X, respectively. Several comments are in order. The AL3X, FACET and FASER (FASER2), which are all detectors in forward region. However, AL3X is closer to the IP than FACET and FASER (FASER2) and has larger size and thus has better sensitivity. The very forward FACET and FASER (FASER2) have weaker sensitivity. They are in general more sensitive to the case where the BSM particles are produced forwardly which is not the case for $H_5^{\pm\pm}$ in current analysis. The MoEDAL-MAPP1 and CODEX-b are two detectors located near the LHCb. For MoEDAL-MAPP1, due to its small size and long distance from IP, it only covers the mass range of $m_5 \in (50, 135)$ GeV. However, for CODEX-b, its size and distance from IP are moderate among all these detectors, the coverage in mass extends to $m_5 \in (50, 160) \,\text{GeV}$. The MATHUSLA and ANUBIS detectors have much better sensitivity as they are large in size and close to the IP. Besides, the ANUBIS is closer to the IP than that of MATHUSLA, hence the exclusion region is shifted towards lower (larger) $c\tau$ (s_H) compared with that of MATHUSLA. Furthermore, the boundaries of the exclusion region follow well with the contours of $c\tau$ of $H_5^{\pm\pm}$ shown in Fig. 3 with an extension at low mass region due to its much larger cross section.

IV. CONCLUSION

The GM model extends SM model with real and complex triplets. The introduction of the complex triplet results in the doubly charged scalar $H_5^{\pm\pm}$ after EWSB. Currently the

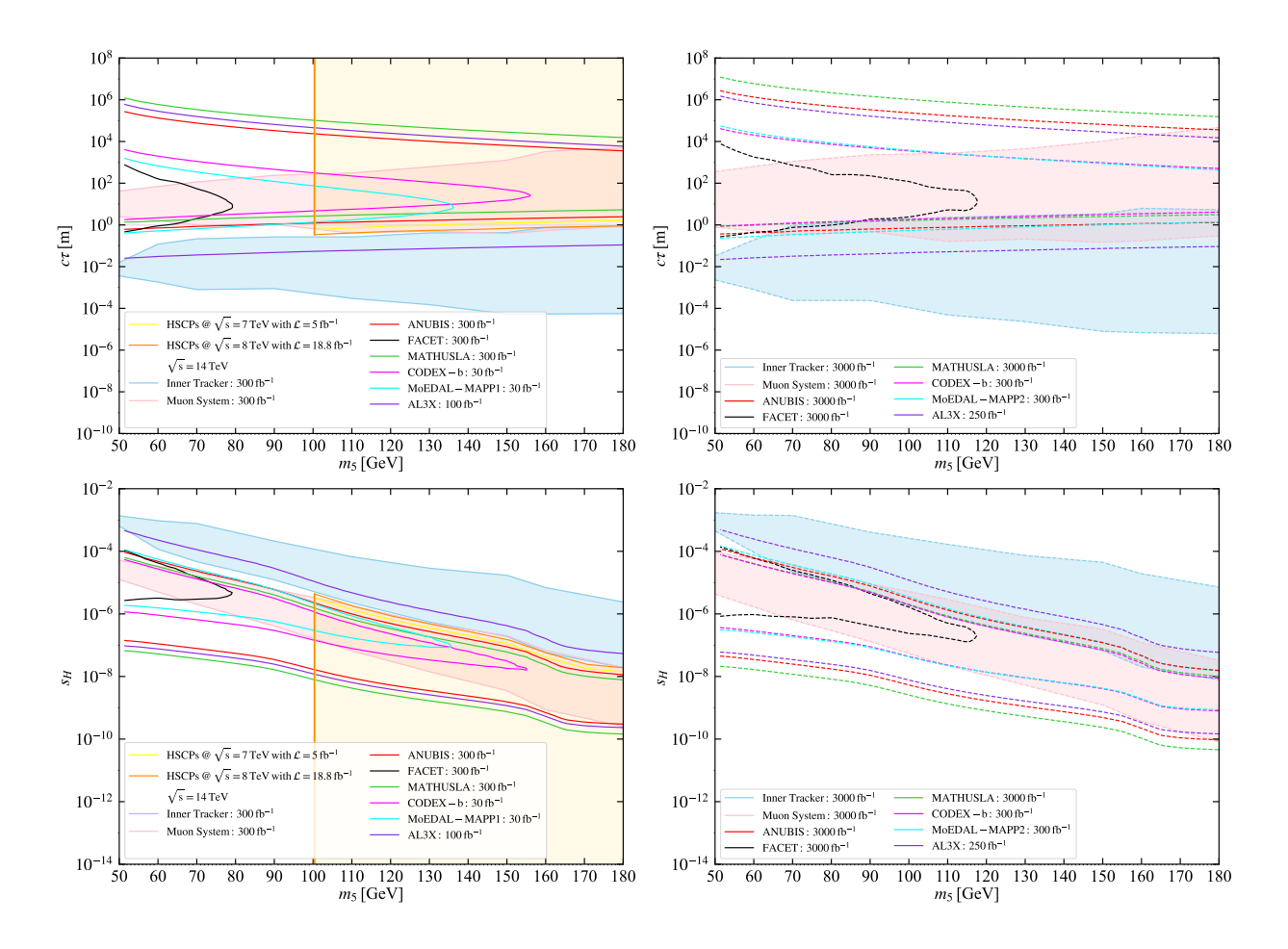


FIG. 8. The 95% C.L. exclusion region for the search of long-lived $H_5^{\pm\pm}$ are shown in the m_5 - $c\tau$ plane at the LHC (upper-left) and the HL-LHC (upper-right), as well as in the m_5 - s_H plane at the LHC (lower-left) and the HL-LHC (lower-right). Additionally, the analysis of HSCP for $\sqrt{s} = 7$ TeV with $\mathcal{L} = 5$ fb⁻¹ and $\sqrt{s} = 8$ TeV with $\mathcal{L} = 18.8$ fb⁻¹ are also shown in the left panels.

searches for the $H_5^{\pm\pm}$ are mainly focusing on high mass regions. However, the $c\tau$ of $H_5^{\pm\pm}$ increases with the decrease of both m_5 and s_H . Hence in the low-mass and low- s_H region, the $H_5^{\pm\pm}$ can become long-lived, where the current searches at colliders mainly depending on the prompt final states signal are no longer applicable. In this work, we thus focus on such region where the doubly charged scalar is long-lived, and consider several different channels to cover the parameter region.

The searches can be categorized according to the lifetime of $H_5^{\pm\pm}$. When the lifetime is short, it may dominantly decay within the inner tracker, leaving displaced vertices for its charged decay products. For simplicity, we consider only the same-sign leptonic channel. The analysis for hadronic final states will be similar. Such channel can cover $c\tau$ from about

 $\mathcal{O}(10^{-4})$ meter to $\mathcal{O}(1)$ meter. Currently analysis assumes fixed selection rules for the charged leptons. Hence, the sensitivity is a bit weaker at lower mass where the leptons are also softer.

When the lifetime gets longer, $H_5^{\pm\pm}$ may travel through the innner tracker and the calorimeters and decay inside the muon system. For this case, we considered the CSC detector of the muon system. All decay products except muons, neutrinos will be reconstructed as the *CSC cluster* while the muon will be isolated as a charged track in the CSC detector. We consider all cases with different number of reconstructed *CSC cluster* and pair of same-sign muons. Combining all these cases, the searches can cover $c\tau$ from $\mathcal{O}(1)$ meter to $\mathcal{O}(100)$ meters.

If the lifetime of $H_5^{\pm\pm}$ is even longer, it may transverse the whole detector before it decays leaving charged track and be called HSCP. Such analysis relies heavily on the simulation of detector response to the charged particles transversing the detector which is beyond the scope of current work. However, by recasting the 7/8 TeV CMS results, we found that the searches for HSCP are powerful enough to cover the entire parameter space for a given mass, where the $c\tau$ is larger than several meters. Translating into the parameter space of GM model, it can cover, for given mass, the scenario that extremely closes to the alignment limit in the GM model, which shows an important complementarity to the other searches at the LHC which can push the parameter space into the alignment limit.

Recently, there has been increasing interest in placing detectors far from the interaction point to detect weakly interacting BSM particles. When $H_5^{\pm\pm}$ leaves the detector, it may also induce signals at various far detectors. In the analysis, we considered MATHUSLA, ANUBIS, FACET, FASER, CODEX-b and MoEDAL-MAPP and AL3X. We found that the exclusion area is influenced by the combined effect of the relative position of far detectors and IP, the size of the far detectors, the integrated luminosity, the decay time of detected particles and the cross-section. For the very forward facilities(FACET and FASER), the sensitivity is weak due to the small acceptance area of these detectors. In HL-LHC, the far detectors around the central region, MATHUSLA, ANUBIS, CODEX-b and MoEDAL-MAPP, the coverage extends from several meters to $\mathcal{O}(10^4)$ meters.

Note that, in current analysis, we didn't consider the case where $H_5^{\pm\pm}$ decays within the calorimeters, which requires a dedicated simulation. However, from Fig. 8, we find that, beside some small gap in the low mass region, the searches from inner tracker, muon system

and HSCP can already cover the whole parameter region that leads to a long-lived $H_5^{\pm\pm}$ in the GM model.

Searches for long-lived particles play an important role in covering the parameter space of the GM model. The usual direct searches generally cover parameter space with large s_H (or equivalently large triplet vev v_{χ}), the model can always escape the stringent constraints by pushing to the alignment limit ($s_H \to 0$). However, the searches for long-lived particles alter the situation. It can cover the parameter space around the alignment limit and hence will be a powerful complimentarity to the usual searches covering the whole parameter space of the GM model.

ACKNOWLEDGMENTS

We would like to thank Zeren Simon Wang for helpful discussion on details of DDC. C.-T. Lu and X. Wei are supported the National Natural Science Foundation of China (NNSFC) under grant No. 12335005 and the Special funds for postdoctoral overseas recruitment, Ministry of Education of China. X. Wang and Y. Wu are supported by the NNSFC under grant No. 12305112.

Appendix A: Trajectories of particles affected by magnetic fields in the LHC detectors

Given a particle with momentum (E, p_x, p_y, p_z) , charge q and a magnetic field aligned along z-axis, the motion of such particle can be described as a combination of two movements: movement with constant velocity along z-axis and circular movement in the transverse x-y plane. Assuming that the strength of the magnetic field is B, the radius of the trajectory in the transverse plane is given by

$$R = \frac{p_T}{qB},\tag{A1}$$

where $p_T = \sqrt{p_x^2 + p_y^2}$. Then the coordinates of the charged particle as functions of time are given by

$$x = \frac{2p_T}{qB}\sin\left(\frac{qBt}{2E}\right)\sin\left(\frac{qBt}{2E} + \frac{\pi}{2} - \theta_0\right),\tag{A2}$$

$$y = \frac{2p_T}{qB} \sin\left(\frac{qBt}{2E}\right) \cos\left(\frac{qBt}{2E} + \frac{\pi}{2} - \theta_0\right),\tag{A3}$$

$$z = \frac{p_z}{E}t,\tag{A4}$$

where θ_0 is the angle between the momentum and the x-axis in the transverse plane at the beginning.

- [1] T. Robens and T. Stefaniak, Status of the Higgs Singlet Extension of the Standard Model after LHC Run 1, Eur. Phys. J. C 75 (2015) 104 [1501.02234].
- [2] L. Wang, J.M. Yang, Y. Zhang, P. Zhu and R. Zhu, A Concise Review on Some Higgs-Related New Physics Models in Light of Current Experiments, Universe 9 (2023) 178 [2302.05719].
- [3] T.D. Lee, A Theory of Spontaneous T Violation, Phys. Rev. D 8 (1973) 1226.
- [4] G.C. Branco, P.M. Ferreira, L. Lavoura, M.N. Rebelo, M. Sher and J.P. Silva, *Theory and phenomenology of two-Higgs-doublet models*, *Phys. Rept.* **516** (2012) 1 [1106.0034].
- [5] L. Wang, J.M. Yang and Y. Zhang, Two-Higgs-doublet models in light of current experiments: a brief review, Commun. Theor. Phys. 74 (2022) 097202 [2203.07244].
- [6] J.F. Gunion, R. Vega and J. Wudka, *Higgs triplets in the standard model*, *Phys. Rev. D* **42** (1990) 1673.
- [7] C. Englert, E. Re and M. Spannowsky, Triplet Higgs boson collider phenomenology after the LHC, Phys. Rev. D 87 (2013) 095014 [1302.6505].
- [8] H. Georgi and M. Machacek, DOUBLY CHARGED HIGGS BOSONS, Nucl. Phys. B 262 (1985) 463.
- [9] M.S. Chanowitz and M. Golden, Higgs Boson Triplets With $M(W) = M(Z) \cos \theta \omega$, Phys. Lett. B 165 (1985) 105.
- [10] C.-W. Chiang, S. Kanemura and K. Yagyu, Novel constraint on the parameter space of the georgi-machacek model with current lhc data, Physical Review D 90 (2014) 115025.

- [11] C.-W. Chiang, G. Cottin and O. Eberhardt, Global fits in the georgi-machacek model, Physical review d 99 (2019) 015001.
- [12] X.K. Du, Z. Li, F. Wang and Y.K. Zhang, Explaining the cdf-ii w-boson mass anomaly in the georgi-machacek extension models, The European Physical Journal C 83 (2023) 1.
- [13] X.K. Du and F. Wang, Positive definiteness constraints of effective scalar potential in georgi-machacek model, arXiv preprint arXiv:2409.20198 (2024).
- [14] H. Sun, X. Luo, W. Wei and T. Liu, Searching for the doubly-charged higgs bosons in the georgi-machacek model at the electron-proton colliders, Physical Review D 96 (2017) 095003.
- [15] D. Das and I. Saha, Cornering variants of the Georgi-Machacek model using Higgs precision data, Phys. Rev. D 98 (2018) 095010 [1811.00979].
- [16] M. Chakraborti, D. Das, N. Ghosh, S. Mukherjee and I. Saha, New physics implications of vector boson fusion searches exemplified through the Georgi-Machacek model, Phys. Rev. D 109 (2024) 015016 [2308.02384].
- [17] A. Kundu, P. Mondal and P.B. Pal, Custodial symmetry, the Georgi-Machacek model, and other scalar extensions, Phys. Rev. D 105 (2022) 115026 [2111.14195].
- [18] D. Chowdhury, P. Mondal and S. Samanta, Next-to-Leading Order Unitarity Fits in the Extended Georgi-Machacek Model, 2404.18996.
- [19] Z. Bairi and A. Ahriche, More constraints on the Georgi-Machacek model, Phys. Rev. D 108 (2023) 055028 [2207.00142].
- [20] A. Ahriche, Constraining the Georgi-Machacek model with a light Higgs boson, Phys. Rev. D 107 (2023) 015006 [2212.11579].
- [21] ATLAS collaboration, Search for resonant WZ production in the fully leptonic final state in proton-proton collisions at √s = 13 TeV with the ATLAS detector, Eur. Phys. J. C 83 (2023) 633 [2207.03925].
- [22] CMS collaboration, Search for charged Higgs bosons produced in vector boson fusion processes and decaying into vector boson pairs in proton-proton collisions at √s = 13 TeV, Eur. Phys. J. C 81 (2021) 723 [2104.04762].
- [23] CMS collaboration, Search for anomalous electroweak production of vector boson pairs in association with two jets in proton-proton collisions at 13 TeV, Phys. Lett. B 798 (2019) 134985 [1905.07445].

- [24] ATLAS collaboration, Search for heavy resonances decaying into WW in the $e\nu\mu\nu$ final state in pp collisions at $\sqrt{s} = 13$ TeV with the ATLAS detector, Eur. Phys. J. C 78 (2018) 24 [1710.01123].
- [25] ATLAS collaboration, Search for a Charged Higgs Boson Produced in the Vector-Boson Fusion Mode with Decay $H^{\pm} \to W^{\pm}Z$ using pp Collisions at $\sqrt{s} = 8$ TeV with the ATLAS Experiment, Phys. Rev. Lett. 114 (2015) 231801 [1503.04233].
- [26] H.E. Logan and Y. Wu, Searching for the $W\gamma$ decay of a charged Higgs boson, JHEP 11 (2018) 121 [1809.09127].
- [27] F. Richard, A Georgi-Machacek Interpretation of the Associate Production of a Neutral Scalar with Mass around 151 GeV, in ILC Workshop on Potential Experiments, 12, 2021 [2112.07982].
- [28] T.-K. Chen, C.-W. Chiang, C.-T. Huang and B.-Q. Lu, Updated constraints on the Georgi-Machacek model and its electroweak phase transition and associated gravitational waves, Phys. Rev. D 106 (2022) 055019 [2205.02064].
- [29] L. Bian, H.-K. Guo, Y. Wu and R. Zhou, Gravitational wave and collider searches for electroweak symmetry breaking patterns, Phys. Rev. D 101 (2020) 035011 [1906.11664].
- [30] A. Ahriche, The 95 GeV Excess in the Georgi-Machacek Model: Single or Twin Peak Resonance, 2312.10484.
- [31] ATLAS collaboration, Search for a light CP-odd Higgs boson decaying into a pair of τ -leptons in proton-proton collisions at $\sqrt{s} = 13$ TeV with the ATLAS detector, 2409.20381.
- [32] ATLAS collaboration, Search for $t\bar{t}H/A \to t\bar{t}t\bar{t}$ production in proton-proton collisions at $\sqrt{s} = 13$ TeV with the ATLAS detector, 2408.17164.
- [33] ATLAS collaboration, Search for heavy neutral Higgs bosons decaying into a top quark pair in 140 fb⁻¹ of proton-proton collision data at √s = 13 TeV with the ATLAS detector, JHEP 08 (2024) 013 [2404.18986].
- [34] ATLAS collaboration, Interpretations of the ATLAS measurements of Higgs boson production and decay rates and differential cross-sections in pp collisions at $\sqrt{s} = 13$ TeV, 2402.05742.
- [35] ATLAS collaboration, Search for a CP-odd Higgs boson decaying into a heavy CP-even Higgs boson and a Z boson in the $\ell^+\ell^- t\bar{t}$ and $\nu\bar{\nu}b\bar{b}$ final states using 140 fb⁻¹ of data

- collected with the ATLAS detector, JHEP **02** (2024) 197 [2311.04033].
- [36] ATLAS collaboration, Search for Higgs boson pair production in association with a vector boson in pp collisions at √s = 13 TeV with the ATLAS detector, Eur. Phys. J. C 83 (2023) 519 [2210.05415].
- [37] ATLAS collaboration, Combined measurements of Higgs boson production and decay using up to 80 fb⁻¹ of proton-proton collision data at $\sqrt{s} = 13$ TeV collected with the ATLAS experiment, Phys. Rev. D 101 (2020) 012002 [1909.02845].
- [38] ATLAS collaboration, Search for heavy neutral Higgs bosons produced in association with b-quarks and decaying into b-quarks at √s = 13 TeV with the ATLAS detector, Phys. Rev. D 102 (2020) 032004 [1907.02749].
- [39] CMS collaboration, Search for new Higgs bosons via same-sign top quark pair production in association with a jet in proton-proton collisions at √s = 13 TeV, Phys. Lett. B 850 (2024) 138478 [2311.03261].
- [40] CMS collaboration, Search for a heavy Higgs boson decaying to a pair of W bosons in proton-proton collisions at $\sqrt{s} = 13$ TeV, JHEP **03** (2020) 034 [1912.01594].
- [41] CMS collaboration, Combined measurements of Higgs boson couplings in proton-proton collisions at $\sqrt{s} = 13$ TeV, Eur. Phys. J. C **79** (2019) 421 [1809.10733].
- [42] ATLAS collaboration, Search for doubly and singly charged Higgs bosons decaying into vector bosons in multi-lepton final states with the ATLAS detector using proton-proton collisions at √s = 13 TeV, JHEP 06 (2021) 146 [2101.11961].
- [43] ATLAS collaboration, Search for doubly- and singly-charged Higgs bosons decaying into vector bosons in multi-leptons final states with the ATLAS detector using proton-proton collisions at $\sqrt{s} = 13$ TeV, ATLAS-CONF-2020-056.
- [44] ATLAS collaboration, Combination of searches for singly and doubly charged Higgs bosons produced via vector-boson fusion in proton-proton collisions at $\sqrt{s} = 13$ TeV with the ATLAS detector, 2407.10798.
- [45] CMS collaboration, A Search for a Doubly-Charged Higgs Boson in pp Collisions at $\sqrt{s} = 7$ TeV, Eur. Phys. J. C 72 (2012) 2189 [1207.2666].
- [46] ATLAS collaboration, Search for doubly charged Higgs boson production in multi-lepton final states using 139 fb⁻¹ of proton-proton collisions at √s = 13 TeV with the ATLAS detector, Eur. Phys. J. C 83 (2023) 605 [2211.07505].

- [47] M.M. Altakach, P. Lamba, R. Masełek, V.A. Mitsou and K. Sakurai, Discovery prospects for long-lived multiply charged particles at the lhc, The European Physical Journal C 82 (2022) 1.
- [48] V. Mitsou, Looking for charged detector-stable particles at the lhc, in Corfu Summer Institute 2023" School and Workshops on Elementary Particle Physics and Gravity", p. 112, 2024.
- [49] H1 collaboration, Search for doubly-charged Higgs boson production at HERA, Phys. Lett. B 638 (2006) 432 [hep-ex/0604027].
- [50] L3 collaboration, Search for doubly charged Higgs bosons at LEP, Phys. Lett. B 576 (2003) 18 [hep-ex/0309076].
- [51] OPAL collaboration, Search for the single production of doubly charged Higgs bosons and constraints on their couplings from Bhabha scattering, Phys. Lett. B 577 (2003) 93 [hep-ex/0308052].
- [52] DELPHI collaboration, Search for doubly charged Higgs bosons at LEP-2, Phys. Lett. B552 (2003) 127 [hep-ex/0303026].
- [53] OPAL collaboration, Search for doubly charged Higgs bosons with the OPAL detector at LEP, Phys. Lett. B **526** (2002) 221 [hep-ex/0111059].
- [54] T. Han, B. Mukhopadhyaya, Z. Si and K. Wang, Pair production of doubly-charged scalars: Neutrino mass constraints and signals at the LHC, Phys. Rev. D 76 (2007) 075013 [0706.0441].
- [55] P.S. Bhupal Dev and Y. Zhang, Displaced vertex signatures of doubly charged scalars in the type-II seesaw and its left-right extensions, JHEP 10 (2018) 199 [1808.00943].
- [56] S. Antusch, O. Fischer, A. Hammad and C. Scherb, Low scale type II seesaw: Present constraints and prospects for displaced vertex searches, JHEP 02 (2019) 157 [1811.03476].
- [57] E. Akhmedov, P.S.B. Dev, S. Jana and R.N. Mohapatra, Long-lived doubly charged scalars in the left-right symmetric model: Catalyzed nuclear fusion and collider implications, Phys. Lett. B 852 (2024) 138616 [2401.15145].
- [58] CMS collaboration, Search for long-lived particles that decay into final states containing two electrons or two muons in proton-proton collisions at $\sqrt{s} = 8$ TeV, Phys. Rev. D 91 (2015) 052012 [1411.6977].

- [59] J.Y. Araz, B. Fuks, M.D. Goodsell and M. Utsch, Recasting LHC searches for long-lived particles with MadAnalysis 5, Eur. Phys. J. C 82 (2022) 597 [2112.05163].
- [60] CMS collaboration, Search for Long-Lived Particles Decaying in the CMS End Cap Muon Detectors in Proton-Proton Collisions at √s =13 TeV, Phys. Rev. Lett. 127 (2021) 261804 [2107.04838].
- [61] M. Bauer, O. Brandt, L. Lee and C. Ohm, ANUBIS: Proposal to search for long-lived neutral particles in CERN service shafts, 1909.13022.
- [62] MATHUSLA collaboration, An Update to the Letter of Intent for MATHUSLA: Search for Long-Lived Particles at the HL-LHC, 2009.01693.
- [63] S. Cerci et al., FACET: A new long-lived particle detector in the very forward region of the CMS experiment, JHEP 06 (2022) 110 [2201.00019].
- [64] FASER collaboration, FASER's physics reach for long-lived particles, Phys. Rev. D 99 (2019) 095011 [1811.12522].
- [65] V.V. Gligorov, S. Knapen, M. Papucci and D.J. Robinson, Searching for Long-lived Particles: A Compact Detector for Exotics at LHCb, Phys. Rev. D 97 (2018) 015023 [1708.09395].
- [66] J.L. Pinfold, The MoEDAL Experiment at the LHC—A Progress Report, Universe 5 (2019) 47.
- [67] V.V. Gligorov, S. Knapen, B. Nachman, M. Papucci and D.J. Robinson, Leveraging the ALICE/L3 cavern for long-lived particle searches, Phys. Rev. D 99 (2019) 015023 [1810.03636].
- [68] K. Hartling, K. Kumar and H.E. Logan, The decoupling limit in the Georgi-Machacek model, Phys. Rev. D 90 (2014) 015007 [1404.2640].
- [69] M. Aoki and S. Kanemura, Unitarity bounds in the Higgs model including triplet fields with custodial symmetry, Phys. Rev. D 77 (2008) 095009 [0712.4053].
- [70] P.S. Bhupal Dev, D.K. Ghosh, N. Okada and I. Saha, 125 GeV Higgs Boson and the Type-II Seesaw Model, JHEP 03 (2013) 150 [1301.3453].
- [71] M. Muhlleitner and M. Spira, A Note on doubly charged Higgs pair production at hadron colliders, Phys. Rev. D 68 (2003) 117701 [hep-ph/0305288].
- [72] P. Fileviez Perez, T. Han, G.-Y. Huang, T. Li and K. Wang, Testing a Neutrino Mass Generation Mechanism at the LHC, Phys. Rev. D 78 (2008) 071301 [0803.3450].

- [73] A. Ismail, B. Keeshan, H.E. Logan and Y. Wu, Benchmark for LHC searches for low-mass custodial fiveplet scalars in the Georgi-Machacek model, Phys. Rev. D 103 (2021) 095010 [2003.05536].
- [74] K. Hartling, K. Kumar and H.E. Logan, GMCALC: a calculator for the Georgi-Machacek model, 1412.7387.
- [75] J. Alwall, M. Herquet, F. Maltoni, O. Mattelaer and T. Stelzer, MadGraph 5: Going Beyond, JHEP 06 (2011) 128 [1106.0522].
- [76] A. Peterson, H. Logan, K. Hartling, K. Kumar and Y. Wu. https://feynrules.irmp.ucl.ac.be/wiki/GeorgiMachacekModel.
- [77] NNPDF collaboration, Parton distributions from high-precision collider data, Eur. Phys. J. C 77 (2017) 663 [1706.00428].
- [78] NNPDF collaboration, Illuminating the photon content of the proton within a global PDF analysis, SciPost Phys. 5 (2018) 008 [1712.07053].
- [79] A. Manohar, P. Nason, G.P. Salam and G. Zanderighi, How bright is the proton? A precise determination of the photon parton distribution function, Phys. Rev. Lett. 117 (2016) 242002 [1607.04266].
- [80] A.V. Manohar, P. Nason, G.P. Salam and G. Zanderighi, The Photon Content of the Proton, JHEP 12 (2017) 046 [1708.01256].
- [81] H.-S. Shao and D. d'Enterria, gamma-UPC: automated generation of exclusive photon-photon processes in ultraperipheral proton and nuclear collisions with varying form factors, JHEP 09 (2022) 248 [2207.03012].
- [82] CMS collaboration, Observation of electroweak production of same-sign W boson pairs in the two jet and two same-sign lepton final state in proton-proton collisions at $\sqrt{s} = 13$ TeV, Phys. Rev. Lett. 120 (2018) 081801 [1709.05822].
- [83] J.C. Romao and S. Andringa, Vector boson decays of the Higgs boson, Eur. Phys. J. C 7 (1999) 631 [hep-ph/9807536].
- [84] HDECAY collaboration, eHDECAY: an Implementation of the Higgs Effective Lagrangian into HDECAY, Comput. Phys. Commun. 185 (2014) 3412 [1403.3381].
- [85] A. Ismail, H.E. Logan and Y. Wu, Updated constraints on the Georgi-Machacek model from LHC Run 2, 2003.02272.

- [86] ATLAS collaboration, Search for Scalar Diphoton Resonances in the Mass Range 65 − 600 GeV with the ATLAS Detector in pp Collision Data at √s = 8 TeV, Phys. Rev. Lett. 113 (2014) 171801 [1407.6583].
- [87] ATLAS collaboration, Search for boosted diphoton resonances in the 10 to 70 GeV mass range using 138 fb⁻¹ of 13 TeV pp collisions with the ATLAS detector, JHEP **07** (2023) 155 [2211.04172].
- [88] CMS collaboration, Search for a standard model-like Higgs boson in the mass range between 70 and 110 GeV in the diphoton final state in proton-proton collisions at $\sqrt{s} = 8$ and 13 TeV, Phys. Lett. B **793** (2019) 320 [1811.08459].
- [89] CMS collaboration, Updated measurements of the Higgs boson at 125 GeV in the two photon decay channel, CMS-PAS-HIG-13-001.
- [90] L. Lee, C. Ohm, A. Soffer and T.-T. Yu, Collider Searches for Long-Lived Particles Beyond the Standard Model, Prog. Part. Nucl. Phys. 106 (2019) 210 [1810.12602].
- [91] T. Sjöstrand, S. Ask, J.R. Christiansen, R. Corke, N. Desai, P. Ilten et al., An introduction to PYTHIA 8.2, Comput. Phys. Commun. 191 (2015) 159 [1410.3012].
- [92] J.Y. Araz, B. Fuks and G. Polykratis, Simplified fast detector simulation in MADANALYSIS 5, Eur. Phys. J. C 81 (2021) 329 [2006.09387].
- [93] E. Conte, B. Fuks and G. Serret, MadAnalysis 5, A User-Friendly Framework for Collider Phenomenology, Comput. Phys. Commun. 184 (2013) 222 [1206.1599].
- [94] E. Conte, B. Dumont, B. Fuks and C. Wymant, Designing and recasting LHC analyses with MadAnalysis 5, Eur. Phys. J. C 74 (2014) 3103 [1405.3982].
- [95] B. Dumont, B. Fuks, S. Kraml, S. Bein, G. Chalons, E. Conte et al., Toward a public analysis database for LHC new physics searches using MADANALYSIS 5, Eur. Phys. J. C 75 (2015) 56 [1407.3278].
- [96] E. Conte and B. Fuks, Confronting new physics theories to LHC data with MADANALYSIS5, Int. J. Mod. Phys. A 33 (2018) 1830027 [1808.00480].
- [97] J.Y. Araz, M. Frank and B. Fuks, Reinterpreting the results of the LHC with MadAnalysis 5: uncertainties and higher-luminosity estimates, Eur. Phys. J. C 80 (2020) 531 [1910.11418].
- [98] A. Mitridate, M. Papucci, C.W. Wang, C. Peña and S. Xie, Energetic long-lived particles in the cms muon chambers, Physical Review D 108 (2023) 055040.

- [99] CMS collaboration, The CMS muon project: Technical Design Report, CERN-LHCC-97-032, CMS-TDR-3.
- [100] CMS collaboration, The CMS Experiment at the CERN LHC, JINST 3 (2008) S08004.
- [101] G. Cottin, J.C. Helo, M. Hirsch, C. Peña, C. Wang and S. Xie, Long-lived heavy neutral leptons with a displaced shower signature at CMS, JHEP 02 (2023) 011 [2210.17446].
- [102] W. Liu, S. Kulkarni and F.F. Deppisch, Revealing the origin of neutrino masses through displaced shower searches in the cms muon system, arXiv preprint arXiv:2407.20676 (2024)
- [103] S. Chatrchyan, V. Khachatryan, A. Sirunyan, A. Tumasyan, W. Adam, T. Bergauer et al., Searches for long-lived charged particles in pp collisions at sqrt s = 7 and 8 tev, Journal of High Energy Physics 2013 (2013).
- [104] C. collaboration et al., Constraints on the pmssm, amsb model and on other models from the search for long-lived charged particles in proton-proton collisions at sqrt (s)= 8 tev, arXiv preprint arXiv:1502.02522 (2015).
- [105] CMS collaboration, Constraints on the pMSSM, AMSB model and on other models from the search for long-lived charged particles in proton-proton collisions at sqrt(s) = 8 TeV, Eur. Phys. J. C 75 (2015) 325 [1502.02522].
- [106] CMS collaboration, Searches for Long-Lived Charged Particles in pp Collisions at \sqrt{s} =7 and 8 TeV, JHEP 07 (2013) 122 [1305.0491].
- [107] MATHUSLA collaboration, A Letter of Intent for MATHUSLA: A Dedicated Displaced Vertex Detector above ATLAS or CMS., 1811.00927.
- [108] ANUBIS collaboration, Searches for long-lived particles with the ANUBIS experiment, PoS EPS-HEP2023 (2024) 051 [2401.11604].
- [109] H.K. Dreiner, J.Y. Günther and Z.S. Wang, R-parity violation and light neutralinos at ANUBIS and MAPP, Phys. Rev. D 103 (2021) 075013 [2008.07539].
- [110] F. Domingo, J. Günther, J.S. Kim and Z.S. Wang, A C++ program for estimating detector sensitivities to long-lived particles: Displaced Decay Counter, 2308.07371.
- [111] G. Aielli et al., Expression of interest for the CODEX-b detector, Eur. Phys. J. C 80 (2020) 1177 [1911.00481].
- [112] F.F. Deppisch, S. Kulkarni and W. Liu, Sterile Neutrinos at MAPP in the B-L Model, 11, 2023 [2311.01719].

- [113] M. Kalliokoski, V.A. Mitsou, M. de Montigny, A. Mukhopadhyay, P.-P.A. Ouimet, J. Pinfold et al., Searching for minicharged particles at the energy frontier with the MoEDAL-MAPP experiment at the LHC, JHEP 04 (2024) 137 [2311.02185].
- [114] D. Felea, J. Mamuzic, R. Masełek, N.E. Mavromatos, V.A. Mitsou, J.L. Pinfold et al., Prospects for discovering supersymmetric long-lived particles with MoEDAL, Eur. Phys. J. C 80 (2020) 431 [2001.05980].
- [115] B.S. Acharya, A. De Roeck, J. Ellis, D.K. Ghosh, R. Maselek, G. Panizzo et al., Prospects of searches for long-lived charged particles with MoEDAL, Eur. Phys. J. C 80 (2020) 572 [2004.11305].
- [116] M. Hirsch, R. Masełek and K. Sakurai, Detecting long-lived multi-charged particles in neutrino mass models with MoEDAL, Eur. Phys. J. C 81 (2021) 697 [2103.05644].
- [117] D. Dercks, H.K. Dreiner, M. Hirsch and Z.S. Wang, Long-Lived Fermions at AL3X, Phys. Rev. D 99 (2019) 055020 [1811.01995].